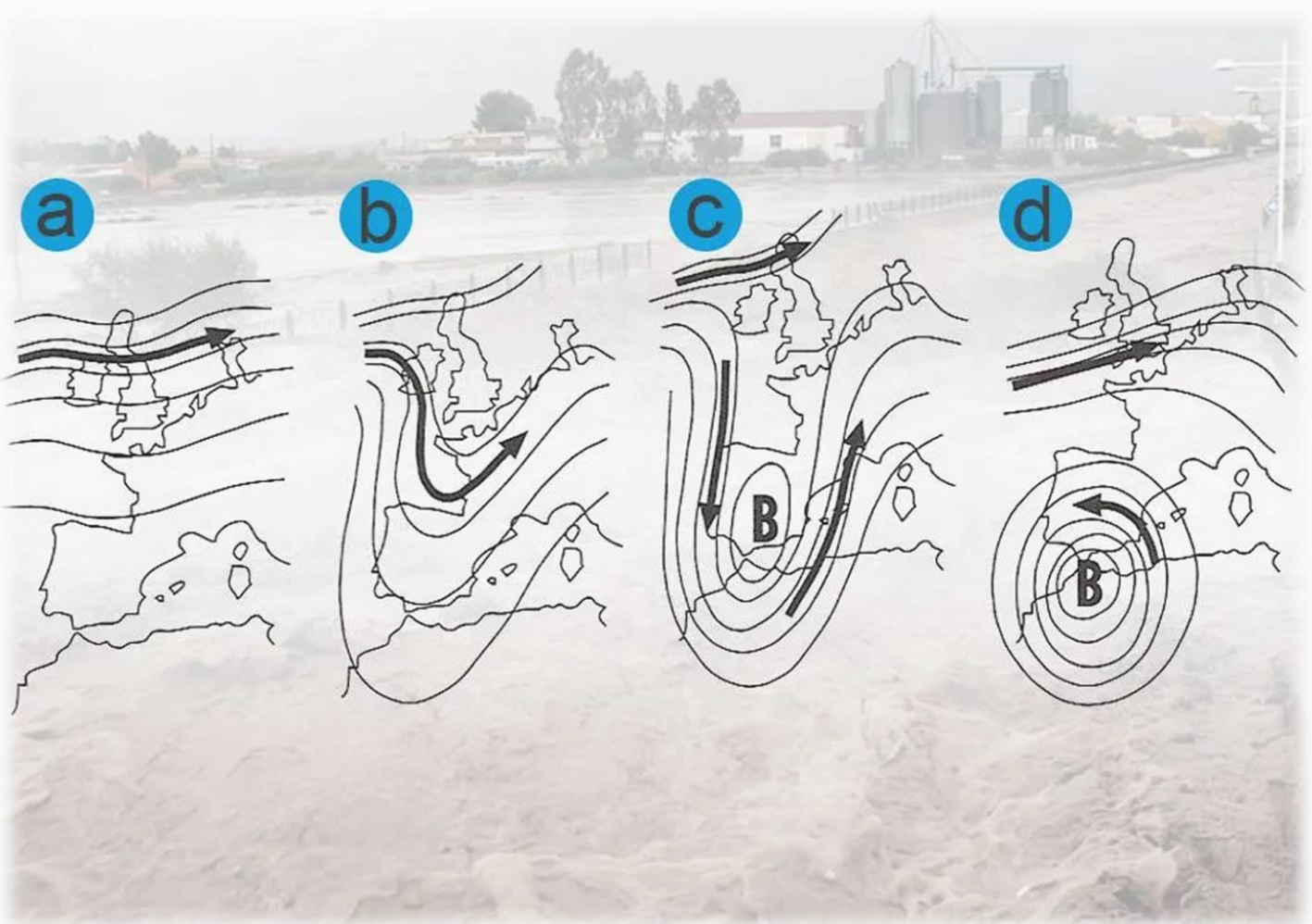


# Cut-off lows and origin of moisture in the Valencia region Spain

MSc thesis - Master Climate Studies



Author: Jelmer Nas (1155652)

Supervisor: Chris Weijenborg

Wageningen University & Research (WUR)

Meteorology and Air Quality (MAQ)

MAQ-80836

2023

# Acknowledgement

During the writing of this thesis, I have received a lot of support and help. My research would have been impossible without the help and support of my supervisor Chris Weijenborg. His expertise, knowledge and useful feedback were crucial for me to set up this research, perform the analyses and write about it in a scientifically way. In particular, the expertise related to python, the Lagrangian trajectory diagnostic LAGRANTO and the diagnostic software tool, called WaterSip, which identifies the evaporative moisture sources based on the output of LAGRANTO helped me a lot.

I am also grateful to my colleagues from my graduation group for providing feedback, support and a positive work attitude during the writing of the thesis.

# Abstract

In Spain, large amounts of precipitation in a short time resulting in flooding are often the result of a “cut-off low”. During the autumn of 1982, 2000, 2012 and 2019, these closed upper-level lows passed south of the Valencia region. These catastrophic weather events resulted in up to 580 mm of precipitation in 24 hours in this region. According to various studies the Mediterranean Sea has a key role in providing the large amounts of precipitation in the Valencia region. This was quantitatively verified in this study.

The ERA-5 reanalysis dataset was used to get an overview of the synoptic situation during the cut-off low events in 1982, 2000, 2012 and 2019. The ERA-5 dataset was compared to the MSWEP dataset. This comparison was done to see if there were spatial differences in precipitation amounts between the datasets. In general, the ERA-5 dataset underestimates the precipitation amounts during the extreme precipitation events. This may have to do with the fact that the precipitation partly consisted of convective precipitation. The ERA-5 dataset was also used to study the atmospheric moisture fluxes, showing the Mediterranean as a possible important source area.

Next, the Lagrangian trajectory diagnostic LAGRANTO was applied to see where the air parcel trajectories came from. The air parcel trajectories were used for the moisture source diagnostic software tool called WaterSip which showed a dominant maritime moisture source from mainly the Mediterranean, but also partly from North Africa (land evaporation).

Due to the changing climate, the most important moisture source - the Mediterranean Sea, will become warmer. This will lead to even more moisture evaporation in the future, resulting in possibly even higher precipitation amounts when a similar event occurs. Based on the results of this study, it is therefore recommended to improve the representation of maritime evaporation in models.

# Contents

1. Introduction.....	5
1.1 Background.....	5
1.2 Problem & Research questions .....	7
1.3 Hypothesis .....	8
2. Methodology .....	9
2.1 Data & methods .....	9
2.2 Model description .....	11
3. Results and discussion.....	14
3.1 Synoptic weather situation .....	14
3.2 Precipitation & validation of ERA-5.....	17
3.3 Air parcel trajectories and moisture transport .....	20
3.4 Evaporative moisture sources.....	22
4. Limitations and recommendations .....	23
4.1 Uncertainties in ERA-5.....	23
4.2 Air parcel trajectories and evaporative moisture sources .....	23
4.3 Temporal and spatial differences in the occurrence of the COL.....	24
5. Conclusion .....	25
References.....	27
Appendix A - Synoptic weather situation.....	32
Appendix B - Air parcel trajectories.....	35
Appendix C – Water vapour fluxes.....	43

# 1. Introduction

## 1.1 Background

The enhanced greenhouse effect on earth is causing the current accelerated climate change and thus a warming climate. Since 1880, the climate has already warmed by about 1°C (CLO, 2018). A warmer world causes more evaporation and thus extra moisture in the atmosphere. The result is also that rainfall amounts are becoming more extreme (IPCC, 2021). This is also the case in Spain, where, in addition to increasingly extreme droughts, floods with significant socio-economic impacts are increasingly occurring (Ferreira, 2021).

### “Cut-Off Lows” in the Valencia region

Heavy precipitation events in a relative short period of time are often the result of a “cut-Off Low” (COL) also known as a “Cold Pool” or “Cold drop” (Awan & Formayer, 2016; Ferreira, 2021). The NOAA’s National Weather Service (n.d.) has defined a COL as “a closed upper-level low (pressure system) which has become completely displaced (or cut off) from basic westerly current (westerlies), and moves independently of that current”. The development of a COL can be seen in Figure 1 and 2. A COL occurs when an “upper level trough” forms. In addition, an essential condition for COL development is the existence of an amplifying synoptic-scale wave in the upper layers of the troposphere. Then the trough deepens, and it starts to detach from the meridional stream. The cold air that is streaming toward the equator is cut off from the general polar flow, and the warm air flowing toward the pole is cut off from the general subtropical flow. Within the southern part of the trough a cold-core, upper-level, low-pressure system is formed. Now a COL has emerged in which the wind blows in a closed circulation. Mainly due to convection, a COL eventually disappears (Nieto et al., 2008).

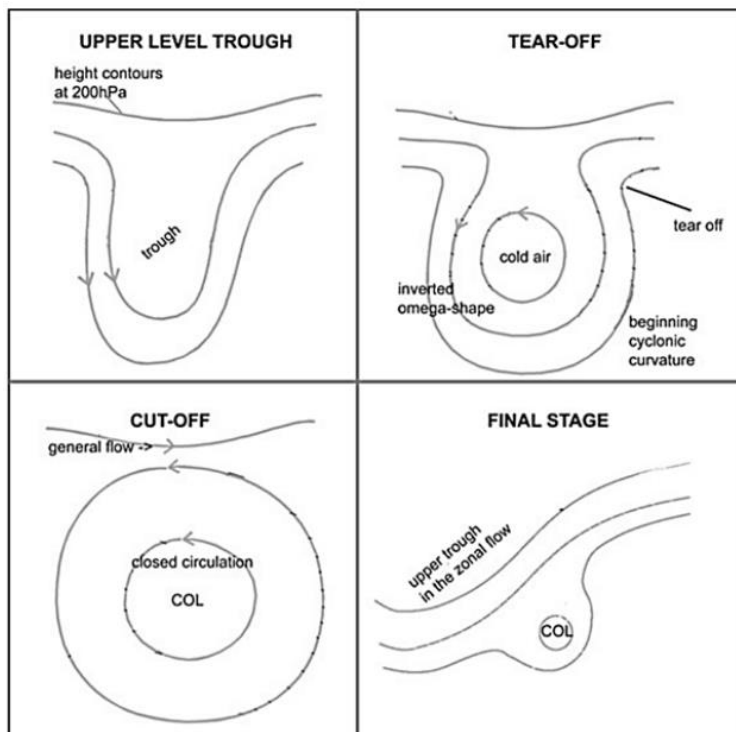


Figure 1: Diagram of the typical synoptic situation of a cut-off low showing the different stages of its life cycle using the geopotential field at 200 hPa (Nieto et al., 2008).



Figure 2: Simplified illustration of the development of a COL (Ocean Navigator, 2017).

COLs can remain almost stationary for days, but can also occasionally move in a westward direction, i.e. in the opposite direction to the flow aloft (retrogression) (NOAA's National Weather Service, n.d.). The air mass in a COL is characterised by warm and moist air at low altitude, while the air at higher altitude is drier and cooler, causing instability. The instability in combination with the slow movement can often cause heavy precipitation events (Tompkins, 2001).

COLs are one of the most important weather systems that affect the southern part of Europe, and are responsible for some of the most catastrophic weather events in terms of precipitation rate (Nieto et al., 2005). The most favoured region in the world for COL occurrence is southern Europe, this is because COLs occur preferentially near the major troughs (elongated region of relatively low atmospheric pressure) of the large-scale circumpolar flow (Nieto et al., 2005). About one third of the most catastrophic floods at the Mediterranean coast of Spain have been shown to be associated with COLs (Ferreira, 2021).

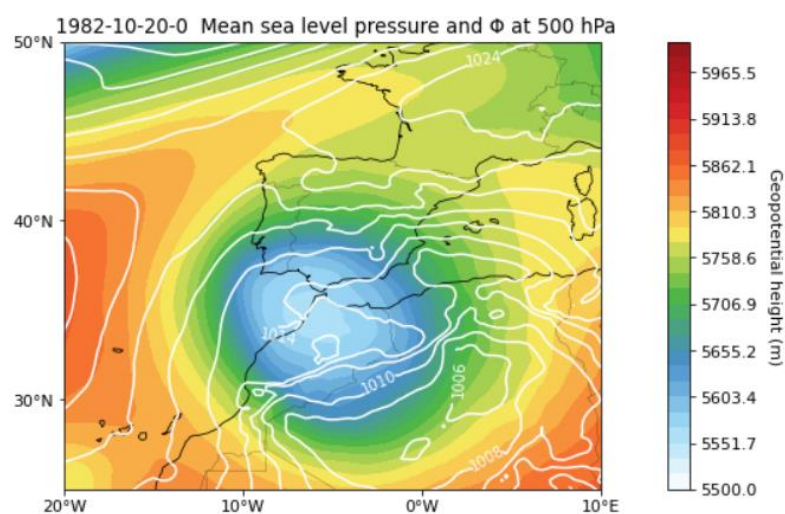


Figure 3: Synoptic situation of the case in October 1982. The COL is situated over Gibraltar and the Northern part of Morocco. The low air pressure (white lines) and low geopotential values (blue colors) indicate cold air layers.

is clearly visible, which remains in this area for several days. An precipitation amount of 580 mm was reported in 24 hours and 69% of the total precipitation fell in only 7 hours (Miró-Granada Gelabert, 2013). Thus, the COL induced precipitation in this example resulted in more precipitation in one day compared to the yearly average in Valencia, which is normally 427 mm in a year (Climate-data.org, n.d.).

More floods have also occurred more recently due to COL systems in the Valencia region. Examples are October 2000, September 2012 and 2019. In 2019 about 300 mm of precipitation fell in only a few days (FloodList News, 2019). Due to the 2019 COL event densely populated cities in the Valencia and Murcia regions flooded, killing 6 people and forcing thousands to evacuate (Ferreira, 2021).

Examples of flood events related to COLs can be found in the Spanish region Valencia, which has endured some of the heaviest flooding caused by COLs. In the region of Valencia COLs produce about 23% of the annual precipitation and 81% of the extreme precipitation (Ferreira, 2021). An example is a case from October 1982 (Figure 3) in which a COL event caused one of the largest floods in the history of that region. An isolated low-pressure area with relatively cold air (shown by the low geopotential



Figure 4 shows the average maximum daily rainfall in a single year, the region of Valencia is the region in Spain that received the largest amounts of precipitation within 24 hours on average. Meaning that it is very sensitive to extreme precipitation within 24 hours. On average, there is one day in each year on which the region received 120 - 140 mm of precipitation, which is strikingly higher compared to the most parts of Spain that received between 30 and 100 mm of precipitation.

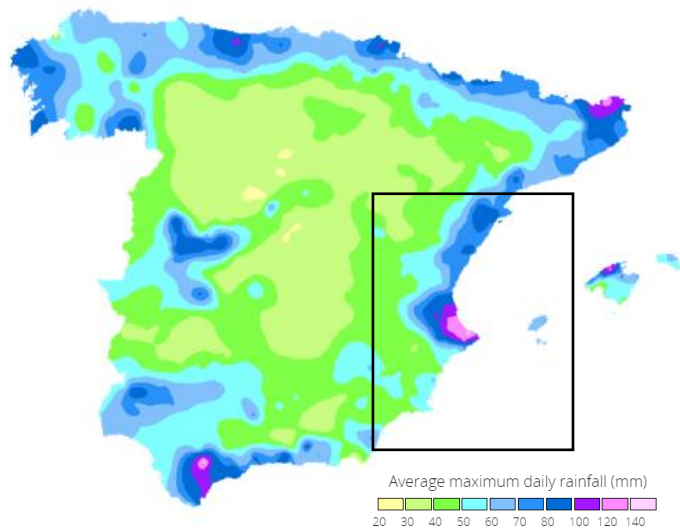


Figure 4: Average maximum daily rainfall (mm) per year, reference period 1981-2010. Black rectangle is the Valencia Region (AEMET, n.d.).

COLs can occur all year-round, especially in spring according to Llasat, Martín, & Barrera (2006). However, COLs in spring almost never cause intense rainfall and flood events. Ferreira (2021) and Llasat, Martín, & Barrera (2006) found that by far most floodings caused by COLs (COL events with largest precipitation amounts) in Spain occur in the autumn (September - November). According to Llasat, Martín, & Barrera (2006) and Ferreira (2021), the Mediterranean Sea has a key role in providing the large amounts of precipitation in the Valencia region. The heavy rainfall is caused by the potential instability associated with the influx of very warm moist air at low levels (and not the influx of cold air at altitude) (Llasat, Martín, & Barrera, 2006). Their analysis of the moisture flux and its convergence in the Valencia region shows that the moisture feeding COL precipitation in the region originated from the Mediterranean Sea. There the specific humidity is large, especially during COL events in autumn, when the seawater temperature is high and the atmospheric stability is low.

## 1.2 Problem & Research questions

Although it seems clear that the Mediterranean Sea is largely responsible for the intense rainfall during several COL events in the Valencia region, it has never been quantitatively verified as far as we know with the lagrangian model LAGRANTO that computes air-parcel trajectories (the route that an air particle (has) traveled in a certain time). Nevertheless, Cloux et al. (2021) did investigate the 1982 case. Using the offline Lagrangian FLEXPART-WRF model, the Western and central Mediterranean appeared to be the main source responsible for the large amount of rain during the October 1982 event. In addition, there are several studies showing that floods caused by a COL elsewhere in Europe have another important source of moisture. For example the study by Smit (2022), here besides the Mediterranean Sea, the Baltic Sea and the European continent, played an important role in providing the moisture.

More extreme precipitation events caused by COLs should be analysed to assess the role and variability of moisture sources (Grams et al., 2014). Also, to improve our ability to predict such floods, it is important to investigate the moisture sources and the transport of it (Grams et al., 2014).

In (North-eastern) Spain extreme COL precipitation could increase by almost 90% and 61% in the Mediterranean region due to a warmer climate (Ferreira, 2021). This makes the source of the evaporative moisture even more important, because the exact origin of precipitation indicates a region's vulnerability to changes in climate and land use, and if it is necessary to improve the representation of ocean or land evaporation in models (Benedict, 2020).

In this study four different case studies (events) within the region of Valencia in Spain are compared (see also the black rectangle in figure 4). Extreme precipitation events occurred in 1982, 2000, 2012 and 2019, and were caused by COLs. The role and variability of the moisture sources are investigated by looking at four cases which caused floodings in the Valencia region due to COLs which took place in 1982, 2000, 2012 and 2019. To investigate the source of the moisture, air parcel trajectories will be created with the Lagrangian Analysis Tool LAGRANTO.

The main research question of this research is:

- *What is the origin of the evaporative moisture sources for the COL induced extreme precipitation events for the four case studies? Is this origin more continental or maritime?*

The research question is broken down to the following sub-questions:

- *What was the exact synoptic weather situation during the COL events, and how did this contribute to generating the precipitation in the Valencia region?*
- *To which extent corresponds the reanalysis dataset (ERA-5) with observational data, considering the spatial patterns of the accumulated precipitation?*
- *What is the relative contribution of advection (large-scale precipitation) and local convection of moisture in a COL event?*

### 1.3 Hypothesis

I expect to confirm the results of the research by Llasat, Martín, & Barrera (2006) and Ferreira (2021) in Spain by quantitatively obtaining the moisture sources in different cases using the lagrangian model LAGRANTO. I thus expect the main source of moisture to come from the Mediterranean Sea. I consider a main source if more than 75 % of the moisture originates from the Mediterranean Sea. Especially since by far the most floods occur in the months of September to November, the period when the seawater is at its warmest. Also, for the Valencia region the heaviest rainfall were in most cases recorded at the eastern or northern edge of a COL system, where the vorticity associated with the pool generated circulation in the lower and middle regions of the troposphere. This meant that the warmer and moist air could reach the region from the Mediterranean Sea (Llasat, Martín, & Barrera, 2006).



## 2. Methodology

This chapter will first discuss the datasets which are used to answer the research questions. It also explain how the four cases are chosen, in addition the area over which the precipitation has fallen and from which the back trajectories will be determined becomes clear. The methods section describes the steps taken in this study. It also goes into more detail about how the research questions can be answered.

### 2.1 Data & methods

#### Case studies & study area

The four chosen case studies are situated in the Valencia region in Spain. The study area of the case studies is simplified with a box of  $38^{\circ}\text{N}$ - $40^{\circ}\text{N}$  x  $1^{\circ}\text{W}$ - $1^{\circ}\text{E}$  as shown in Figure 5. This area is chosen because this is the area which received the heaviest rainfall leading to floodings during the COL events. In addition, from this area it is calculated where the air parcels came from that end up in this area.



Figure 5: Study area for the four case studies (blue rectangle)  $37^{\circ}\text{N}$ - $41^{\circ}\text{N}$  x  $2^{\circ}\text{W}$ - $2^{\circ}\text{E}$  (Racicot, 2022)

In this research the four case studies have been chosen from heavy precipitation events that occurred over the last 42 years (1980-2022). Due to the lack of satellite observations, the observations that were made longer ago are less reliable and are therefore not included in this study (Hersbach et al., 2020). The four case studies (Table 1) are extreme precipitation events caused by COLs and are obtained from the articles made by Ferreira (2021) and Llasat, Martín, & Barrera (2006).

*Table 1: The 4 case studies in the Valencia region, precipitation amounts based on MSWEP data.*

<b>Case study</b>	<b>Year/ Month</b>	<b>duration of COL event (days of month)</b>	<b>Max precipitation (24h)</b>	<b>Max precipitation (whole event)</b>
1	1982 / 10	19 - 21	195 mm	345 mm
2	2000 / 10	20 -24	225 mm	385 mm
3	2012 / 09	27 - 29	105 mm	112 mm
4	2019 / 09	11 -13	200 mm	295 mm

### **ECMWF Reanalysis 5th Generation (ERA-5)**

ERA-5 (meteorological) data is used to get an overview of the synoptic situation during the COL events. Reanalysis data combines a mix of observations with short-range weather forecasts, rerun with current forecasting models using data assimilation (Hersbach et al., 2020). The data from ERA-5 covers the Earth on a 30km grid and resolve the atmosphere using 137 levels from the surface up to a height of 80km.

More specifically, for each single level (surface) data of the following variables will be used; mean sea level pressure; total precipitation (large-scale and convective precipitation); Convective Available Potential Energy (CAPE); temperature at 2 m height; evaporation; vertical integral of both the northward and eastward water vapour flux. Because for COL systems the differences can be large for each pressure level, it is important to also study the data on pressure levels. The dataset on pressure levels has a vertical coverage of 1000 hPa to 1 hPa with a vertical resolution of 37 pressure levels (Copernicus Climate Change Service, 2022). For pressure levels (200, 500 and 850 hPa) hourly data of geopotential height, specific humidity ( $q$ ), zonal wind ( $u$ ), meridional wind ( $v$ ) and the vertical velocity will be used.

ERA-5 data is used to get an overview of the synoptic situation. The synoptic situation of the different case studies will be assessed to obtain a complete and detailed description of the synoptic weather situation and to find out how the large-scale weather pattern of the extreme precipitation events emerged. To understand the flow in different atmospheric layers, the synoptic weather situation of each case will be analysed by investigating the development of the geopotential height at 500 hPa and the mean sea level pressure. The geopotential height at 500 hPa in combination with the temperature at this pressure level will be used to visualise the development of the COL. It is also relevant to compare the effect of the exact positions of the COL systems. It matters, for example, whether a COL system passes north or south from the area (if it will move south than the wind is coming from the Mediterranean). Moreover, in order to answer the second sub-question, analysing the synoptic situation is essential. Data including the variation in large-scale precipitation and convective precipitation, CAPE and the water vapour flux will help in answering this question.

Furthermore ERA-5 data is used to compare precipitation amounts (see next paragraph) and for the backward tracking of air parcels with LAGRANTO. LAGRANTO takes input files of the ERA-5 3-D wind fields (zonal wind  $U$ , meridional wind  $V$  and vertical wind ( $\Omega$ ) at several time steps.

### Multi-Source Weighted-Ensemble Precipitation (MSWEP)

To validate how well ERA-5 is able to reproduce the extreme precipitation, the output of ERA-5 will be compared to observations from MSWEP (Multi-Source Weighted-Ensemble Precipitation). This is a global precipitation product with a 3-hourly 0.1° resolution. The data is available from 1979 until present. The product is unique in the sense that it merges gauge, satellite, and reanalysis data to obtain the highest quality precipitation estimates at every location (land and sea) (GloH20, 2022). A disadvantage of MSWEP is that it also uses reanalysis, and is therefore not completely independent. For this reason, it would have made sense to also use E-OBS (European daily high-resolution gridded dataset). This precipitation dataset is based on interpolation of (only) station data (European Climate Assessment & Dataset, 2022). However, the disadvantage of E-OBS is that it only contains observations on land. This is a big disadvantage, because the region of Valencia is located directly on the Spanish coast. In addition, the time intervals do not match the ERA-5 dataset, therefore in this study only MSWEP will be used to validate extreme precipitation.

ERA-5 data of total precipitation is summed and used for comparison against daily values of MSWEP for the period of the intense rainfall of the case studies (Table 1). The differences in temporal and spatial patterns between the datasets will be studied. Plots of the daily precipitation will be made to visually evaluate spatial differences. We need to make sure that there has been a large amount of rain in the study area.

## 2.2 Model description

### Air parcel trajectories LAGRANTO

For creating air parcel trajectories, the Lagrangian Analysis Tool (LAGRANTO) model is used. LAGRANTO can compute air-parcel (back)trajectories based on the ERA-Interim data on a regular lat/lon grid (Sprenger & Wernli, 2015). The movement of air parcels through space and time can be described by trajectories (Sodemann et al., 2008). With LAGRANTO it is possible to do backward tracking of air parcels using different starting heights in the atmosphere. ERA-5 data on 60 different model levels (from 0 hPa to 1000 hPa) will be used for the backward tracking of air parcels (ECMWF, 2022). LAGRANTO solve numerically the following trajectory equation:

$$\frac{Dx}{Dt} = u(x).$$

Here  $x$  is the position vector in geographical coordinates and  $u$  is in this case the 3-D wind vector. It deals with individual air particles and calculates the trajectory of each particle separately. A large benefit of LAGRANTO is that it makes the starting positions of trajectories very flexible, in addition, a selection of (subsets of) certain trajectories from a larger set is quite easy to make.

In short, LAGRANTO consists of four different steps (see Figure 6). The first step is needed to specify the starting positions of the air parcels. For the four cases (Table 1), the starting positions are all the positions within the study area (Figure 5), and pressure levels from 1000 to 200 hPa with 30 hPa intervals. The next two steps are used for the calculation of the air parcel trajectories and selecting trajectories by applying a filter specified by commands. The last command is used for tracing several meteorological variables along those trajectories. Variables like specific humidity, relative humidity and boundary layer height are important for the moisture attribution which is described in the next section (Sprenger & Wernli, 2015).

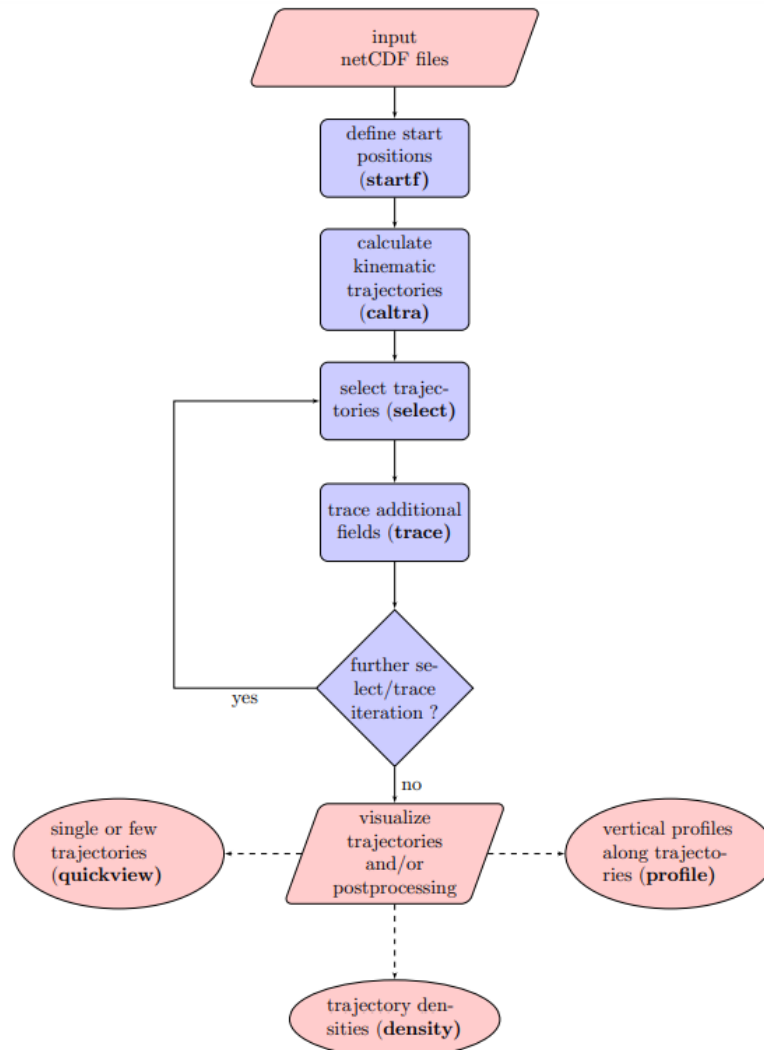


Figure 6: Flowchart showing the typical steps (written in bold in the blue rectangles) in LAGRANTO. Starting positions (longitude, latitude, pressure) are defined with **startf**. Next the trajectories are calculated with **caltra**. With **select** the possibly subsamples of trajectories are selected. With **trace** along these trajectories additional fields are traced. The resulting trajectories can be further analysed or visualized with **quickview**, **density** and **profile** (Sprenger & Wernli, 2015).

### Evaporative moisture sources (WaterSip)

Lastly, to quantify the evaporative moisture sources, the moisture source diagnostic software tool called WaterSip, developed by Sodemann et al., (2008), will be used. The starting positions and starting times of the trajectories are exactly the same as the ones that were used for the air parcel trajectories. For this analysis, 15 day backward trajectories of LAGRANTO with the same horizontal and vertical spacing are used as input for this diagnostic as was also done by Grams et al. (2014).

WaterSip is a software tool that identifies the source, transport and several properties of the atmospheric water vapour based on the backward trajectories. The paper of Sodemann et al., (2008) described the exact calculations done in WaterSip. The two main steps are to identify the moisture uptake locations and the moisture source attribution itself. The interest is to identify the origin of water vapour that leads to precipitation. The first step in this section is therefore to select all air particles that precipitate at the initial time step. For this, it is assumed that precipitation occurs when the relative humidity at the initial time step is 80% or more. Because the moisture changes in an air particle

is generally the net result of precipitation and evaporation, the sign of the change of specific humidity during a certain time interval indicates a location with either evaporation or precipitation.

The second step is to determine the precipitation amount for the initial location of the backward trajectory.

Thirdly, tracing the air parcel backward will be done until a threshold of a positive  $\Delta q_0$  (specific humidity) larger than 0.2 g/kg is being detected. This prevents false uptakes due to numerical errors and also keeps the calculations mathematically feasible.

A moisture source attribution is needed, because earlier moisture uptake locations contribute less to the precipitation at the arrival site (because the air parcels can undergo more than one cycle of evaporation and precipitation within one trajectory). Therefore, the precipitation at the study area is simply a sum weighted of the previous uptake locations. The first step in this calculation is to initialise all the moisture increases at the before determined uptake locations. The next step is to evaluate those unweighted contributions by proceeding forward in time along the backward trajectory. At the starting point, the sum of all the latest fractional contributions of all moisture uptake locations in the boundary layer leads to the fraction of total precipitation to which sources are able to be attributed. Figure 7 shows a conceptual figure of the moisture source attribution method which identifies uptake locations along a backward trajectory of an air parcel.

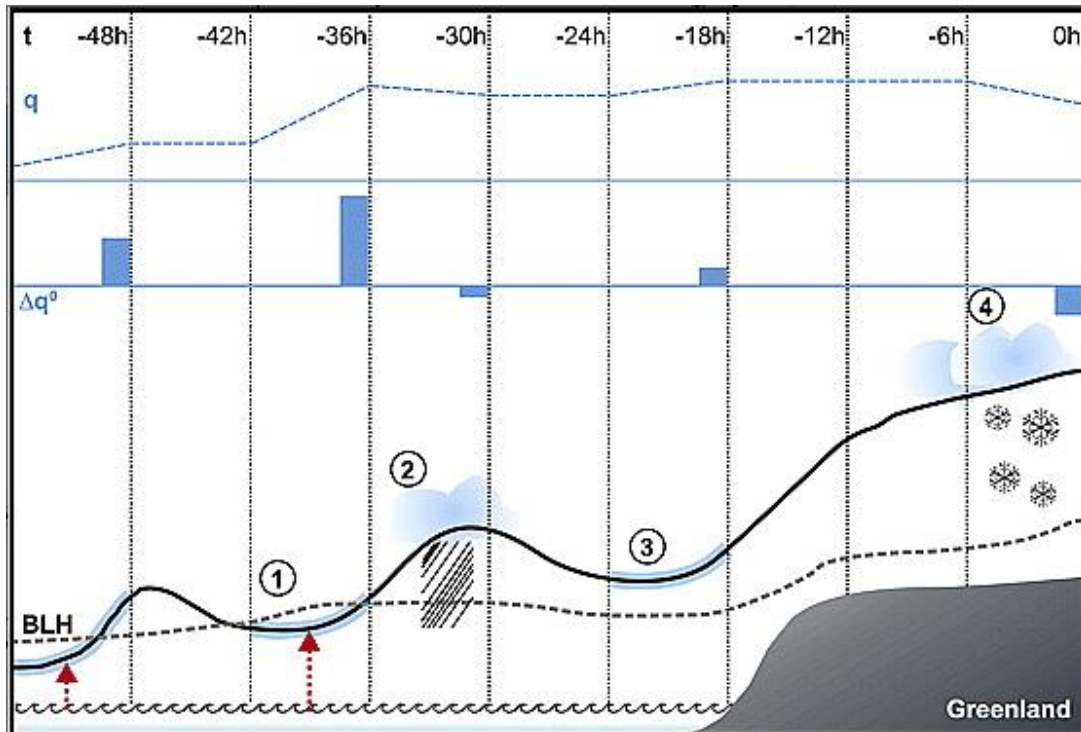


Figure 7: Method for identifying moisture uptakes along a backward trajectory of an air parcel from the Atlantic ocean to Greenland (black line).  $q$  (blue dashed line): Specific humidity in the air parcel (g/ kg).  $\Delta q_0$ : Changes in specific humidity of an air parcel. BLH: Boundary layer height. Thick blue sections along the trajectory: Sections of moisture increase. Red arrows: evaporation locations (Sodemann et al., 2008).



### 3. Results and discussion

#### 3.1 Synoptic weather situation

This section assesses the synoptic situation of the different case studies. The synoptic weather is described in terms of the development of geopotential height at 500 hPa and the mean sea level pressure. The geopotential height at 500 hPa in combination with the temperature at this pressure level will be used to visualise the development of the COL.

The synoptic weather situation over three time steps during the first event (1982) is shown in Figure 8. The other cases are shown in Appendix A. The figure shows that at the 19th of October an intruding upper-level trough above the Atlantic Ocean with relatively cold air is being transported eastward to lower latitudes (Fig 8.a). One day later (Fig 8.b), which is roughly the peak moment of the extreme precipitation event, a closed upper-level circulation has formed shown by the lower geopotential heights at 500 hPa above southern parts of Spain and Morocco compared to the surroundings. The COL is clearly visible and it is completely separated from the main (wavy) jet stream and regular eastward flow. The centre is filled with cold air with temperatures of 250 K (-23°C). Also, in all of the three timesteps (Fig 8.) the development of upper-level ridges (an elongated area of relatively high atmospheric pressure compared to the surrounding environment) to the west, east and north of COL are clearly present, shown by the higher values in geopotential height and temperature. Those high pressure ridges over the Atlantic Ocean, Central- and Eastern Europe lead to blocking and eventually to the stationarity of the COL low over the south of Spain. At the end of the event (Fig 8.c), the size of the COL system becomes gradually smaller and somewhat less cold, indicating a decrease in strength. However, the temperatures are still significantly lower compared to its surroundings and therefore the COL is still assumed to provide energy for large-scale upward moves. At the last day of the event of the 1982 case, the stationarity is even more clear, because it barely changed position and there is still a closed circulation visible.

For the other three events (2000, 2012 and 2019) a comparable development is found (Appendix A). Each event starts with an expanding upper-level trough from the Atlantic Ocean to lower latitudes. Subsequently, a closed upper-level circulation arises, which is the COL. Ridges are present, especially above the Atlantic Ocean and Eastern Europe, which causes the stationarity of the COLs.

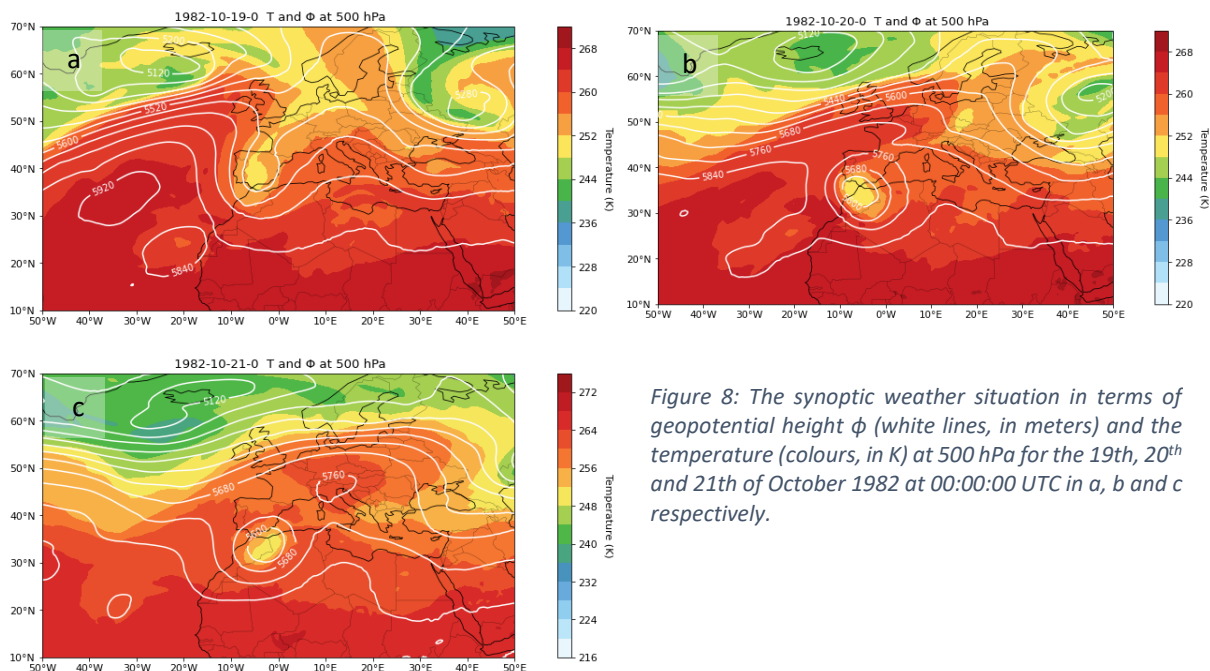


Figure 8: The synoptic weather situation in terms of geopotential height  $\phi$  (white lines, in meters) and the temperature (colours, in K) at 500 hPa for the 19th, 20th and 21th of October 1982 at 00:00:00 UTC in a, b and c respectively.

The upper-level air entered the study area at the start of the four events mainly from the south, changing in the next time steps to more eastern directions, which means that the flow came from the Mediterranean. In Figure 9 (a-d), the geopotential height of the 500 hPa pressure level and the mean sea level pressure at roughly the peak moment of the extreme precipitation events are shown for all the four cases. It shows an eastern flow at 500 hPa for the cases in 1982, 2000 and 2012, whereas for the 2019 case the flow was more from the northeast.

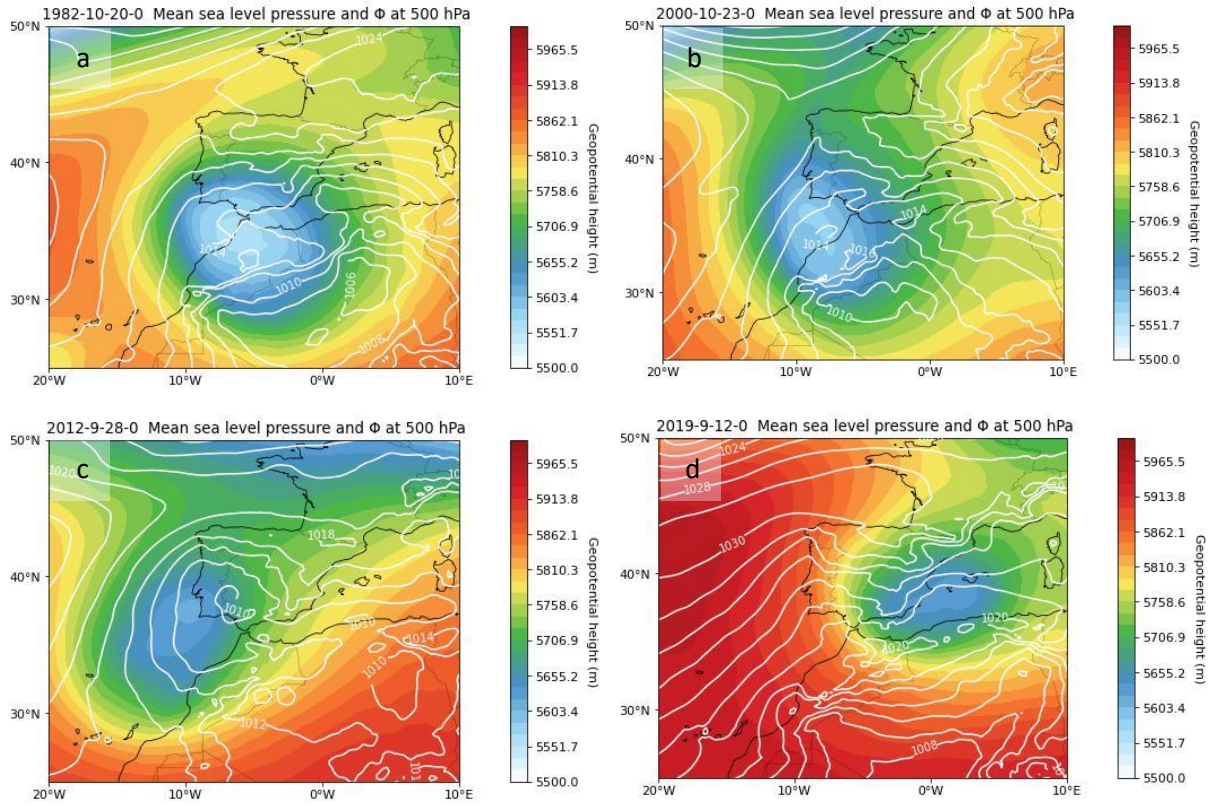


Figure 9: The COL is clearly recognizable in all four cases by the low values of geopotential height ( $\phi$ ). Time step is approximately the peak time of the extreme precipitation event. White lines represents surface pressure, colors geopotential height. 1982, 2000, 2012, 2019 in (a), (b), (c) and (d), respectively.



The moisture transport in terms of the water vapour flux shows at the start of the extreme precipitation events that the circulation is relatively weak compared to the circulation around the COL at the other time steps (Appendix C). In figure 10, the water vapour flux is visualised at the day with the highest precipitation sum. The circulation is counter clockwise around the COL. Following the arrows from the study area backward, reveals that the Mediterranean is an important source area of the air. However, caution is advised given that this only concerns one time step. In this example it is possible to do this since a COL is almost stationary and so the associated wind field is. In addition, the Mediterranean borders directly on the Valencia region. In other cases you would want to have the wind several hours in the past to have a realistic picture of where the wind is coming from. It is noticeable that the air column is most humid over sea, just before the shore. After reaching the land surface, the amount of water vapour decreases rapidly inland direction.

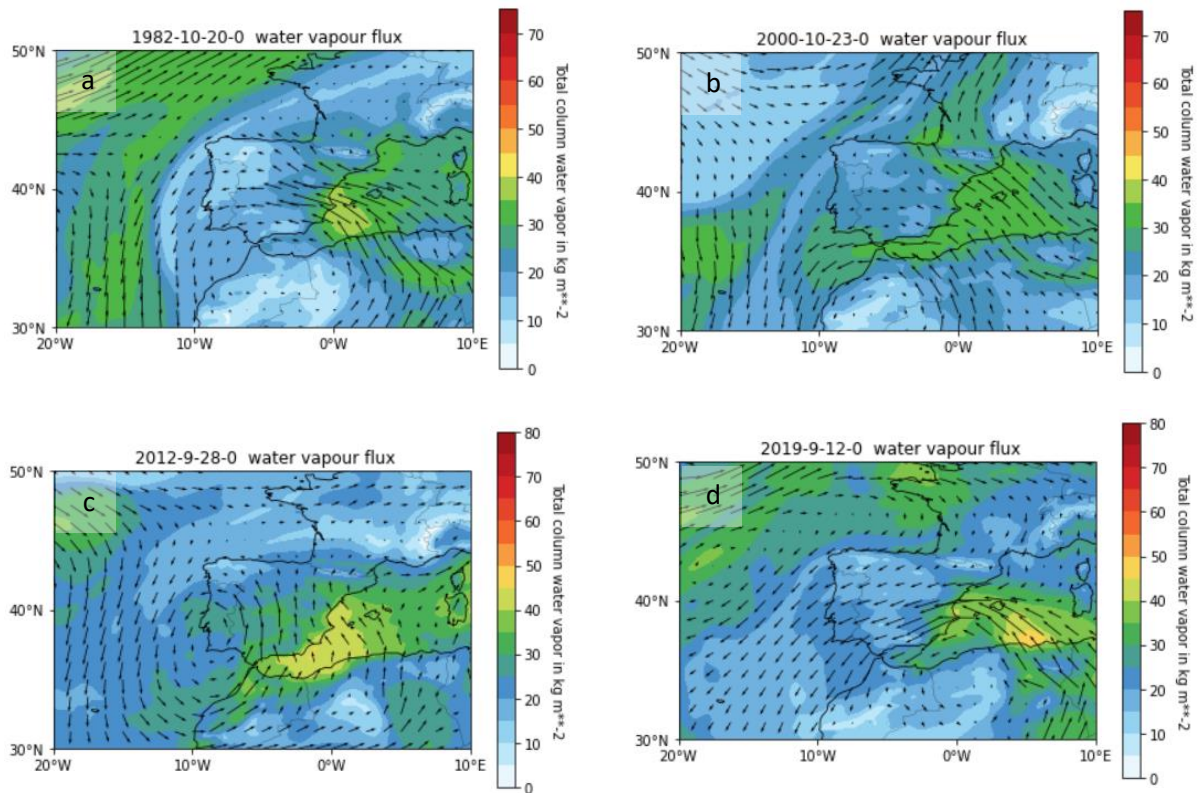


Figure 10: Vertical integral of water vapour flux (arrows) and total column water vapour (colours) over Southwest Europe at 20th of October 1982 00:00 UTC (a), 23<sup>th</sup> of October 2000 00.00 UTC (b), 28th of September 2012 00.00 UTC (c) and 12<sup>th</sup> of September 2019 00.00 UTC (d).

### 3.2 Precipitation & validation of ERA-5

Now we will take a detailed look at the precipitation in the region of Valencia during the events. The precipitation quantities simulated by ERA-5 will be compared with the MSWEP dataset (see 2.1). In addition, a distinction is made between convective and large-scale precipitation. Figure 11 shows the total amount of precipitation per case. In the years 1982 and 2012, precipitation fell on three consecutive days. In 2000 and 2019 this was during four days.

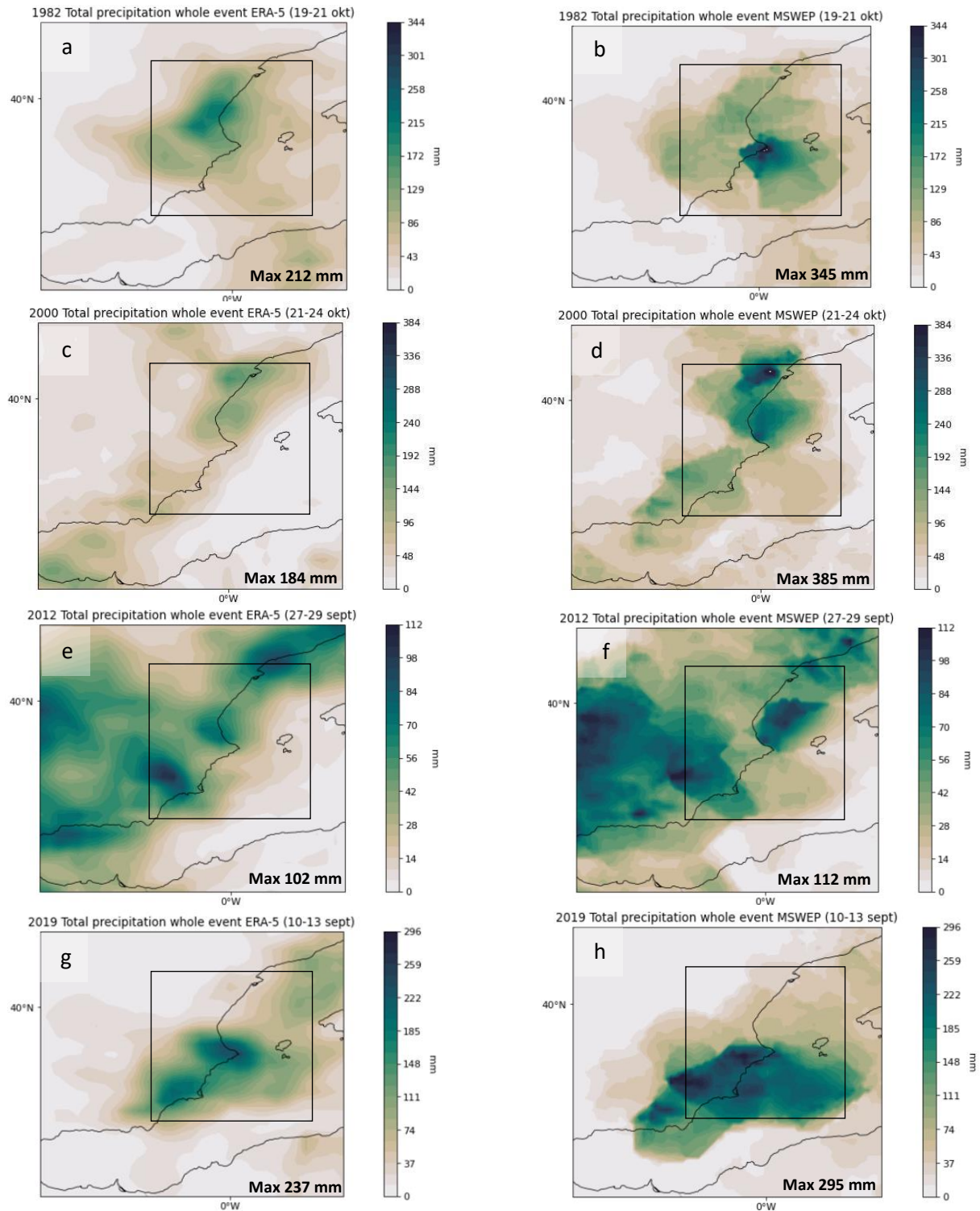


Figure 11: The precipitation sum (in mm) of the period of the four different case studies in the study area (black rectangle) is shown of ERA5 and MSWEP. 19 – 21 October 1982 (a and b), 21 – 24 October 2000 (c and d), 27 – 29 September 2012 (e and f) and 10 – 13 September 2019 (g and h). ERA-5 plots are shown in a, c, e and g. MSWEP plots are shown in b, d, f and h.

Figure 11 shows large deviations in precipitation amounts between ERA-5 and MSWEP. ERA-5 seems to underestimate precipitation in all four cases for the study area. In the most extreme case, the year 2000, the difference in total precipitation is about 200 mm at the location where the most precipitation fell. Based on the MSWEP dataset, which as described earlier consists of gauge, satellite, and reanalysis data, the most precipitation, up to 385 mm in the northeast of the region (Fig 11.d), fell in the year 2000. In second place is the year 1982 with 345 mm of precipitation (Fig 11.b). This time the largest amount of precipitation was in the centre of the study area. Also quite recently in 2019, an amount of almost 300 mm of precipitation fell over mainly the southern part of the region (Fig 11.h). 2012 is by far the case with the least amount of precipitation (up to 112 mm). The more extreme the precipitation amounts, the larger the difference between the two data sets. In Figure 11, it can be found that the location of the most extreme precipitation is mostly more or less the same between the ERA-5 and the MSWEP dataset. In every case the exact location where the most precipitation fell was different from each other. In 1982 most precipitation fell in the middle of the study area (Fig 11. a-b), in 2000 just a little further to the northeast (Fig 11. c-d). In 2012, precipitation was somewhat more spread over the study area (Fig 11. e-f), while in 2019 most precipitation fell further south (Fig 11. g-h).

It is unclear what caused the large deviations in precipitation amounts. As said before, MSWEP is partly based on the interpolation of station data. Errors could partly be due to propagation of errors in station data into the gridded dataset. Also, limitations in the interpolation method or a scarce weather station density network could lead to errors. However, it is unlikely that a scarce weather station network leads to errors, as MSWEP uses satellite and reanalysis data in addition to station data to estimate rainfall amounts. It is more likely that ERA-5 underestimates precipitation amounts. Jiang et al. (2021) found that it is more difficult for ERA-5 to accurately forecast moderate or higher daily precipitation events (above 10 mm/day).

Figure 12 shows that the precipitation that fell during the four cases consists for a large part of convective precipitation. A characteristic of convective precipitation is that the amounts can vary largely from place to place, especially with extreme precipitation amounts. Convection involves multiple processes, many of which take place at scales smaller than the model's grid cell, this requires parameterization (Becker et al., 2019). This makes convective precipitation more difficult to predict than large-scale precipitation. Especially in 1982, 2000 and 2019, the share of convective precipitation was larger than the share of large-scale precipitation. These are also the years in which the precipitation amounts were the most extreme and the data sets deviate quite strongly from each other. In 2012, the share of large-scale precipitation is slightly larger and the difference between the datasets is also the smallest. It is therefore quite plausible that ERA-5 underestimates precipitation.



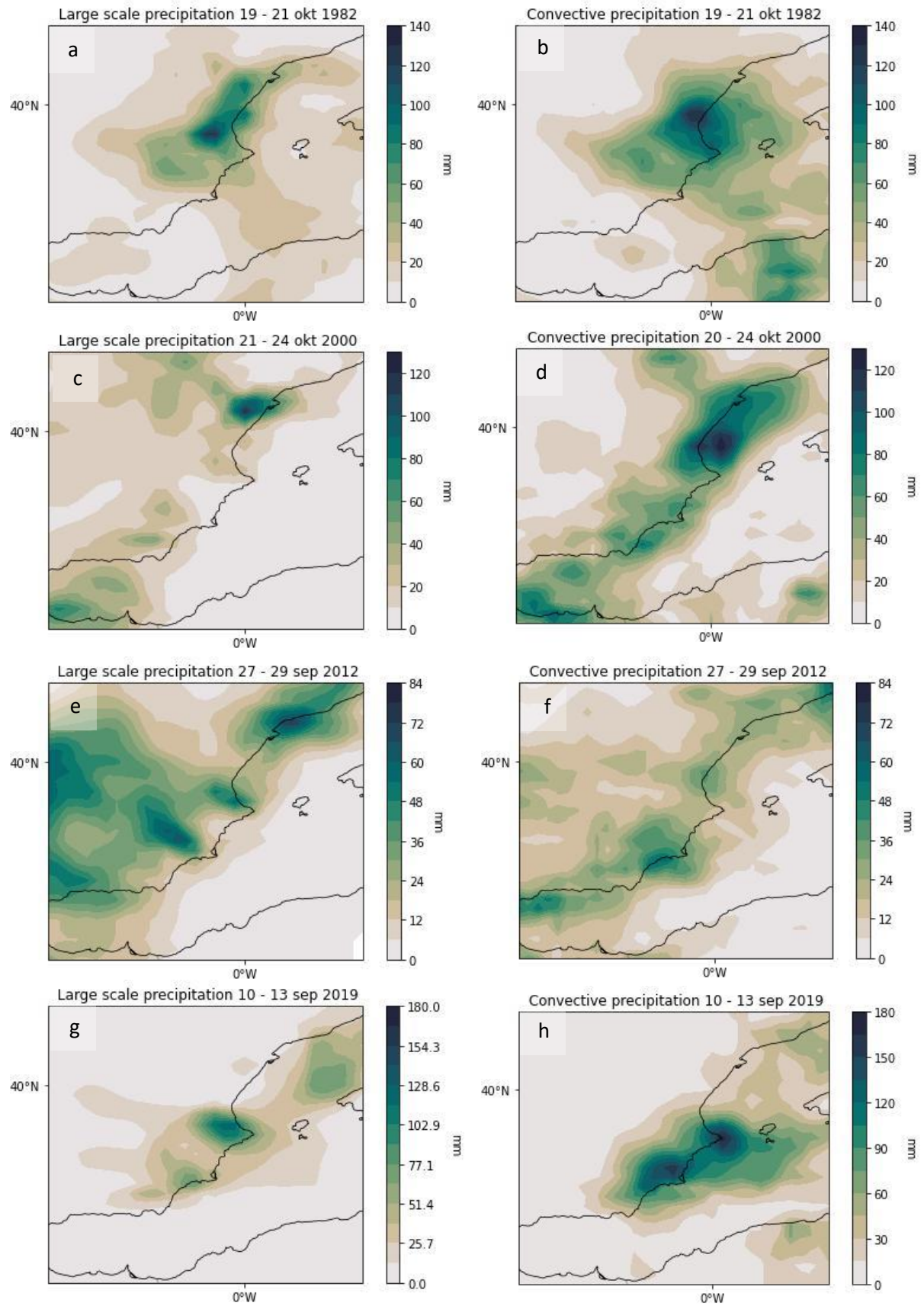


Figure 12: Distribution convective (left) and large scale precipitation (right) based on ERA-5. Large scale precipitation plots are shown in a,c,e and f. Convective precipitation plots are shown in b,d,f and h.

### 3.3 Air parcel trajectories and moisture transport

The air parcel trajectories, which are obtained from LAGRANTO, visualise where the air (holding the moisture) originated from at different atmospheric heights. Only the case of 1982 is shown here over different time steps in figure 13. The 72 hour backward trajectories is visualised in figure 13 for all the four cases. The start time in the figure 13 is the day with the highest precipitation sum. An extensive figure of the trajectories including different starting times can be found in Appendix B for all the four cases. In figure 12 and 13, only the trajectories with an initial relative humidity of 80% or more ( $RH > 80\%$ ) and with a negative difference in specific humidity between two consecutive time steps ( $\Delta q \leq 0$ ) are selected in order to plot only the trajectories which led to precipitation at the starting time (in the study area) as is assumed by Sodemann et al. (2008).

At the beginning of each case (day 1), the air particles mainly enter the study area from the Atlantic Ocean (Fig 13.a and Appendix B). Looking at the surface layer (1050 – 700 hPa), in 1982 and 2012 the air particles originate from the north Atlantic Ocean, approximately between Iceland and Great Britain and lower latitudes (Atlantic Ocean west of Portugal). For the atmosphere at higher altitude (400 - 700 hPa), the air particles in 1982 and 2019 originate mainly from only the lower latitudes (the Atlantic Ocean west of Portugal). For the 2000 case the air parcels are coming from only lower latitudes, this applies in this case to both air layers (1050 - 750 hPa and 400 – 700 hPa). However, in the surface layer we also see air particles that come from the Mediterranean Sea. The pattern of the air parcel trajectories in 2019 are a bit more chaotic during the first time step. Here the trajectories coming from the north are somewhat more divided.

One day later (Fig. 14), roughly the day with the highest precipitation amounts, the air particles mainly come from the Mediterranean Sea. Furthermore, the Atlantic Ocean (west of Portugal) also contributes in 2000 and 2012 (Fig 14.d-f). Especially in 2000, a large difference can be observed between the two different air layers (Fig 14. c-d). While the air particles in the surface layer mainly come from the Mediterranean region, the air particles higher up in the atmosphere especially come from the Atlantic Ocean.

Towards the end of the four events, the Mediterranean remains the main area from which the air particles emerge, however the Atlantic Ocean was an important second source area, especially in 1982 (Fig. 13.c) and 2012 (Appendix B).

It is striking that the air parcel trajectories mainly have the Mediterranean Sea and the Atlantic Ocean as source areas, while the (European) continent is not or hardly regarded as a source area. But it must be said that the trajectories coming from the Mediterranean also come from across North Africa and sometimes the Balkans, see for example figure 14.c. Evaporative moisture source calculations, which will follow, will answer the question where the moisture sources are situated along these trajectories.

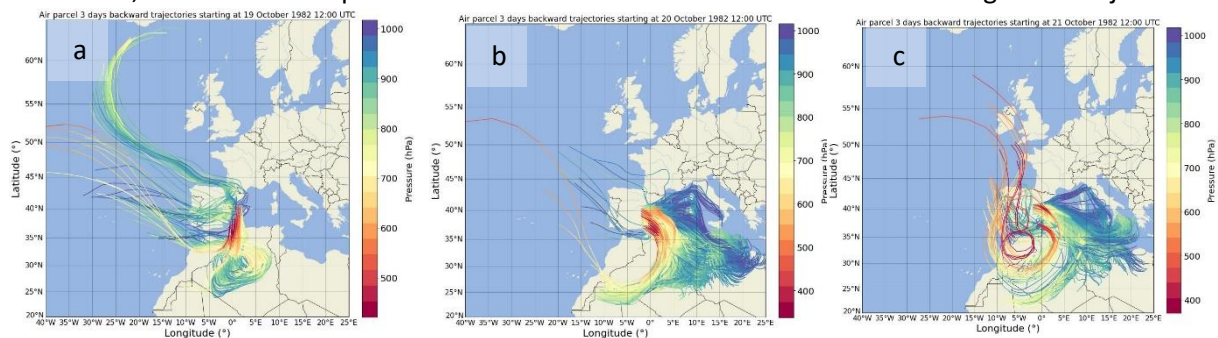


Figure 13: Air parcel 72 hour backward trajectories obtained with LAGRANTO starting at 19th of October 1982 12:00 UTC (a), 20th of October 1982 12:00 UTC (b) and 21th of October 1982 12:00 UTC (c). The pressure indicates the atmospheric height of the air parcel. Only the air parcel trajectories with an initial relative humidity of 80% or more and  $\Delta q \leq 0$  are selected.



700 down to 1050 hPa

400 down to 700 hPa

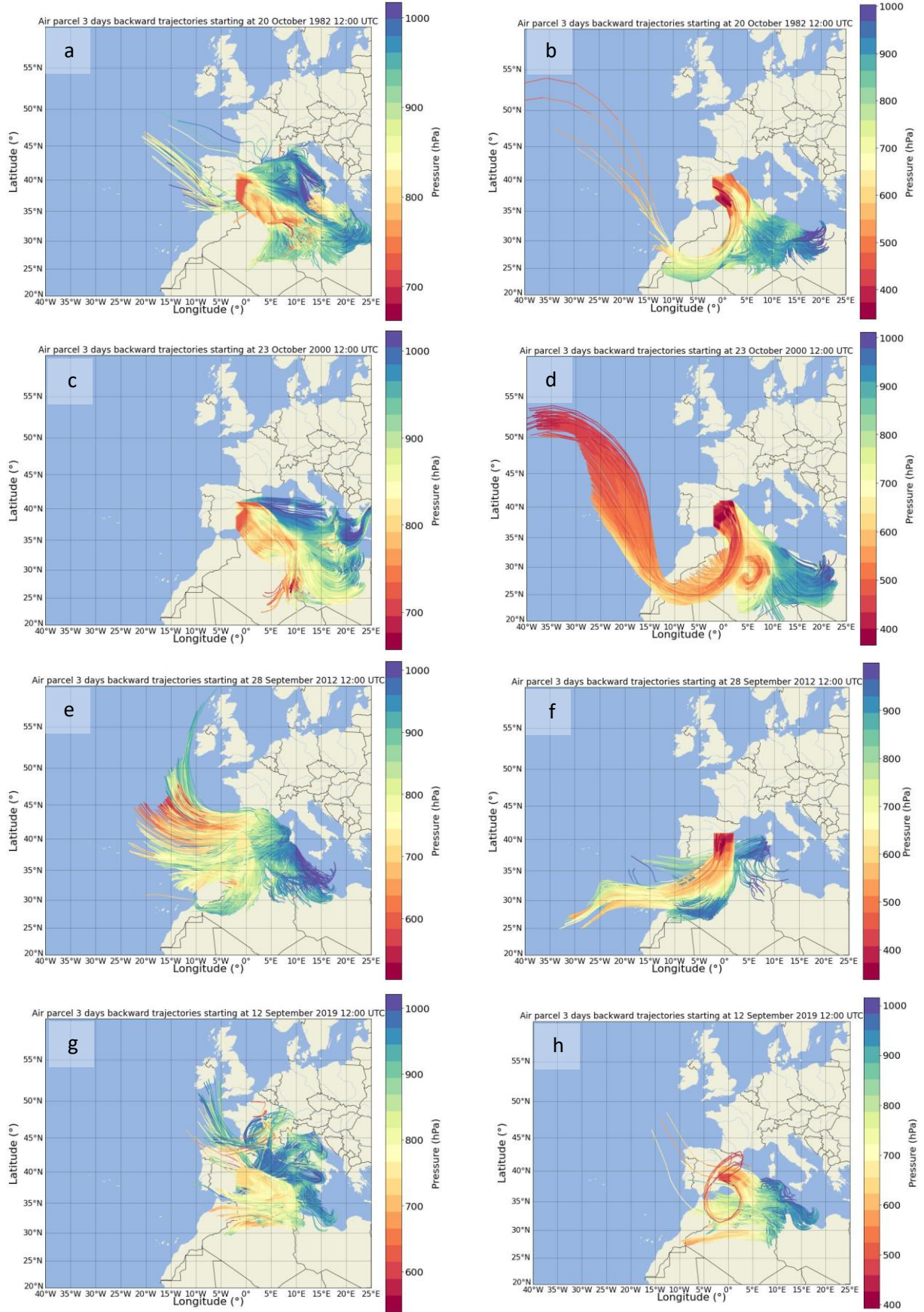


Figure 14: Air parcel 72 hour backward trajectories obtained with LAGRANTO. Time step is roughly the peak of the precipitation. Two different atmospheric layers are visible, 700 to 1050 hPa (left column) and 400 to 700 hPa (right column). Only the air parcel trajectories with an initial relative humidity of 80% or more and  $\Delta q \leq 0$  are selected.

### 3.4 Evaporative moisture sources

This subchapter shows where the moisture that led to precipitation in the study area came from during the four different events. Figure 15 (a-d) shows the locations where the moisture leading to the extreme precipitation came from during the four events. It immediately becomes clear that the four different events have great similarities in terms of the location of the moisture uptake. As expected, most of the moisture clearly comes from the Mediterranean region (maritime evaporation). In particular, the location of the moisture absorption in 1982 and 2000 is almost identical. This mainly concerns the southern Mediterranean. During the events in 2012 and 2019, the area was clearly further east, with the heaviest uptake of moisture around the Balearic Islands (east Mediterranean). However, not only the Mediterranean Sea is responsible for the moisture that led to the extreme precipitation. The north of the African continent (land evaporation) also played an important role as a location for absorbing moisture that led to precipitation and should not be ignored, especially the extreme north of the African continent, roughly the countries of Morocco, Algeria, Tunisia and Libya. This is unexpected, because this was not expected beforehand and are normally relatively dry areas. A reason for this can be that a significant amount of precipitation have fallen prior to the events, which then evaporated. Also Cloux et al. (2021) who investigated the 1982 case found that cloudiness was abundant over most of North Africa, so that some of this water could have evaporated into the very dry Saharan lower atmosphere, leading to an increase in water vapor content. Only an almost negligible amount of moisture originates from the Atlantic Ocean in 1982 and 2012.

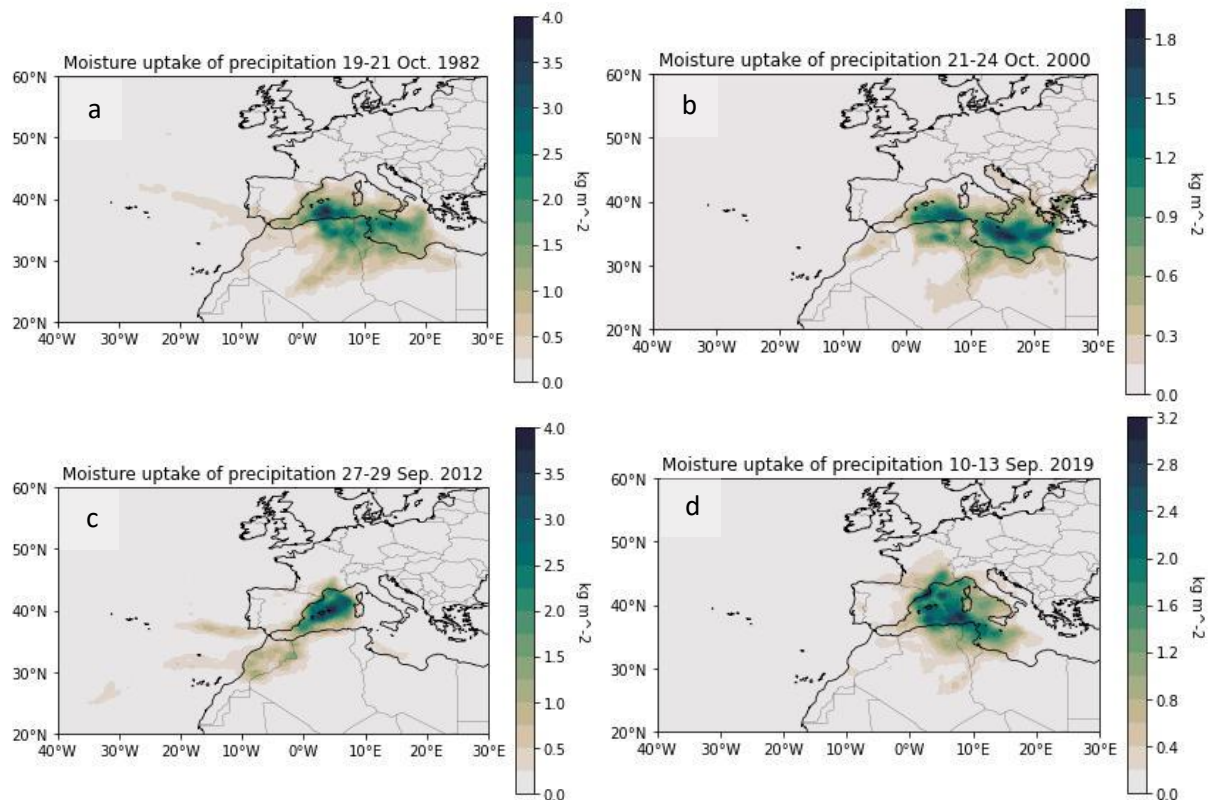


Figure 15: Absolute moisture uptake leading to precipitation within the study area for four different atmospheric layers during the events.



## 4. Limitations and recommendations

### 4.1 Uncertainties in ERA-5

First of all, there are limitations with regard to the ERA-5 reanalysis dataset, which is used for analysing the different case studies. This concerns both the data itself and the methods of this dataset. Uncertainty is an important point of attention here. Reanalysis combines model data with observations, this principle, called data assimilation involves uncertainties. The Ensemble of Data Assimilations (EDA) system takes into account mostly random uncertainties in the observations, for example sea surface temperature and the physical parametrizations of the model (ECMWF, 2023). The most difficult meteorological variable to estimate is precipitation, because of the high spatiotemporal heterogeneity (Beck et al., 2019). In the end, these uncertainties also affect the analyses and results in this study. The horizontal resolution of the ERA-5 dataset is  $0.25^\circ \times 0.25^\circ$  (28 km x 28 km). Data with this resolution can resolve large-scale precipitation events quite well, because the scale of those events is larger than the resolution of the dataset. However, local convection can be too small to be resolved by this dataset. This is probably also what we see when comparing the datasets of ERA-5 and MSWEP. For calculating local convective precipitation, a resolution of 3 km or finer is recommended. A resolution of 7 km is needed to resolve larger convection processes (Fosser et al., 2014). However, the statements regarding the MSWEP dataset should be treated with caution. As mentioned, this is partly generated on the basis of reanalysis data, so the comparison is not completely independent. However, the combination with the station observations and satellite data makes it more reliable, especially because the resolution is significantly higher with  $0.1^\circ \times 0.1^\circ$ . On the other hand, the extreme rainfall boundaries are very sharp, perhaps even too sharp, this is visible in for example figure 11.h, which may make it less reliable. Next to the horizontal resolution, also the used vertical resolution of ERA-5 with a vertical resolution of 50 hPa throughout the whole atmospheric layer (1000 hPa up to 300 hPa) could influence the reliability of the results. This is the case, for example, for the boundary layer, where most of the exchange between surface and atmosphere takes place. 50 hPa is then a fairly high resolution. For further research of these uncertainties, it is recommended to repeat the comparison with a model with a higher resolution to check whether approximately the same precipitation patterns and amounts are found for the four specific cases.

### 4.2 Air parcel trajectories and evaporative moisture sources

The data which is used to create the air parcel trajectories in LAGRANTO is based on ERA-5 data, a direct consequence is that the errors and uncertainties affect the results in LAGRANTO, and thus propagate also further into WaterSip, because data which is used in WaterSip are dependent on the air parcel trajectories data of LAGRANTO.

Another point to mention is that the threshold used for the selection of the air parcel trajectories and to determine the moisture sources is arbitrary. This concerns the thresholds of the trajectories that generate rain at a humidity of more than 80 % ( $RH > 80\%$ ) and a negative difference in specific humidity between two consecutive time steps ( $\Delta q \leq 0$ ). This threshold has been chosen since it was also used in other literature. However, if a different threshold (less strict) was chosen, multiple trajectories would have been selected, possibly resulting in a different interpretation of the moisture sources.

In addition, LAGRANTO was used to calculate the air parcel trajectories. However, if another model than LAGRANTO was chosen to work with in this study, different outcomes in for example the air parcel trajectories and consequently the moisture sources could have occurred. For example the Lagrangian FLEXPART-WRF model could be used. It is also possible to track the moisture sources with an Eulerian approach, for example with the model WAM-2layers. This possibly results in different outcomes. For

these reasons, it is recommended to repeat the analysis with one or more other models, as well as different thresholds used to show only the air parcel trajectories that generate rain. However, I do not expect the results to differ significantly. Most likely is that the Mediterranean remains by far the largest contributor, given the season of the extreme precipitation events and the associated warm sea water. In addition, we found evidence from other studies which are mentioned earlier that have investigated a number of cases.

#### 4.3 Temporal and spatial differences in the occurrence of the COL

Finally, the four different events have been carefully chosen. The COLs in the cases all took place after 1950, caused a lot of precipitation in the Valencia region resulting in flooding and took place in the autumn. In addition, the movement of the cut off lows was also broadly the same. There are (only a few) examples known where COLs in other seasons caused a lot of flooding in eastern Spain, an example is June 2000 (Llasat, Martín, & Barrera, 2006). There are also very likely examples where a COL developed differently and had a different movement, for example north of the study area instead of south. It is recommended to also investigate these cases with LAGRANTO and WaterSip, to see if and to what extent the results differ.

## 5. Conclusion

In Spain, large amounts of precipitation in a short time resulting in flooding are often the result of a “cut-off low”. During the autumn of 1982, 2000, 2012 and 2019, these closed upper-level lows passed south of the Valencia region. These catastrophic weather events resulted in up to 580 mm of precipitation in 24 hours in this region. According to Llasat, Martín, & Barrera (2006) and Ferreira (2021) who researched different COLs in the Valencia region in combination with heavy precipitation amounts, the Mediterranean Sea was the largest contributor to the moisture that caused the large amounts of precipitation. In addition, Cloux et al. (2021) investigated the October 1982 event using an offline Lagrangian model. The result of this study was that the western and central Mediterranean was the main source responsible for the large amount of rain during the October 1982 event. Other studies, including Smit (2022) and a previous thesis study from Thomas Vermeulen that investigated COL cases elsewhere in Europe found the European continent to be an important source of moisture. As far as we know, the COL cases in the Valencia region have never been quantitatively verified with the Lagrangian model LAGRANTO that calculates air parcel trajectories. In this study it is quantified with LAGRANTO for four different COL events during the years 1982, 2000, 2012 and 2019.

The main question in this research is *“What is the origin of the evaporative moisture sources for the COL induced extreme precipitation events for the four case studies? Is this origin more continental or maritime?”* answered using three sub-questions, namely:

- *What was the exact synoptic weather situation during the COL events, and how did this contribute to generating the precipitation in the Valencia region?*
- *To which extent corresponds the reanalysis dataset (ERA-5) with observational data, considering the spatial patterns of the accumulated precipitation?*
- *What is the relative contribution of advection (large-scale precipitation) and local convection of moisture in a COL event?*

To answer the first research question, the ERA-5 reanalysis dataset was used to get an overview of the synoptic situation during the cut off low events in 1982, 2000, 2012 and 2019. At the start of each event an intruding upper-level trough above the Atlantic Ocean with relatively cold air was being transported eastward to lower latitudes, towards the Valencia region. During the peak of the extreme precipitation (around day 2 or 3) the cut off low has formed, with temperatures of around 250 (-23°C) at 500 hPa. The large temperature differences between surface and upper air provides the energy for strong convection and large-scale precipitation near the system. Upper-level ridges to the west, east and north of COL caused the stationarity of the COLs. Because the core of the COL is situated south(west) of the Valencia region, the wind came from eastern directions, which means that the flow came from the Mediterranean. The study of atmospheric moisture fluxes shows the Mediterranean as a potentially important source area.

The second and third sub-question were addressed in Chapter 3.2. *Precipitation & validation of ERA-5*. The ERA-5 dataset was compared to the MSWEP dataset, this comparison was done to see if there were spatial differences in precipitation amounts between the datasets. In general, the ERA-5 dataset underestimates the precipitation amounts during the extreme precipitation events, the difference is in the most extreme case 200 mm between the two data sets. The more extreme the precipitation amounts, the larger the difference between the two data sets. This may have to do with the fact that the precipitation partly consisted of convective precipitation. A characteristic of convective precipitation is that the amounts can vary largely from place to place, especially with extreme precipitation amounts. This makes convective precipitation more difficult to predict than large-scale precipitation. In 1982, 2000 and 2019, the share of convective precipitation was larger than the share

of large-scale precipitation. These are also the years in which the precipitation amounts are the most extreme and the data sets deviate quite strongly from each other.

To answer the main question, first the Lagrangian trajectory diagnostic LAGRANTO was used to calculate where the air parcel trajectories came from. Here, too, there are great similarities between the four events. At the beginning of the events the air particles originated from the Atlantic Ocean. Approximately one day later, roughly the day with the highest precipitation amounts, the air particles mainly came from the Mediterranean. We also see great similarities between different air layers. Only in 2000 there was a major difference in the origin of air parcels between air parcels higher up in the atmosphere and air parcels at the surface during extreme precipitation. The air parcel trajectories were used for the moisture source diagnostic software tool called WaterSip which showed a dominant maritime moisture source from mainly the Mediterranean, but also partly from North Africa (land evaporation).

Nevertheless, there are some points of attention with regard to the reliability of this study that should be taken into account. This concerns in particular the uncertainties and the resolution with regard to the ERA-5 reanalysis data set (28 km x 28 km). Deze resolutie is te klein om convectieve neerslag goed te kunnen berekenen/ voorspellen. a resolution between 3 km and 7 km is needed to resolve larger convection processes (Fosser et al., 2014). Also the chosen threshold used for the selection of the air parcel trajectories and to determine the moisture sources is arbitrary. For further research I recommend to repeat the comparison of precipitation data with a higher resolution dataset to see if the same rainfall patterns and amounts are found for the four specific cases. In addition it is recommend to repeat the analyses of this study with a different model and different thresholds to see if and how this differs.

## References

- Awan, N. K., & Formayer, H. (2016, March 15). *Cutoff low systems and their relevance to large-scale extreme precipitation in the European Alps*. SpringerLink. Retrieved September 20, 2022, from [https://link.springer.com/article/10.1007/s00704-016-1767-0?error=cookies\\_not\\_supported&code=9633e6c1-cec9-407a-ab7a-99b6e713bed2](https://link.springer.com/article/10.1007/s00704-016-1767-0?error=cookies_not_supported&code=9633e6c1-cec9-407a-ab7a-99b6e713bed2)
- Becker, T., Bechtold, P., & Sandu, I. (2019, November 12). Modelling convective precipitation – progress and challenges. ECMWF. Retrieved June 15, 2023, from <https://www.ecmwf.int/en/about/media-centre/science-blog/2019/modelling-convective-precipitation-progress-and-challenges#:~:text=Convection%20is%20complex%20and%20hard,systematic%20errors%20in%20convective%20precipitation.>
- Beck, H. E., Wood, E. F., Pan, M., Fisher, C. K., Miralles, D. G., Van Dijk, A., McVicar, T. R., & Adler, R. F. (2019). MSWEP V2 Global 3-Hourly 0.1° Precipitation: Methodology and Quantitative Assessment. *Bulletin of the American Meteorological Society*, 100(3), 473–500. <https://doi.org/10.1175/bams-d-17-0138.1>
- Benedict, I. B. (2020). Atmospheric moisture transport and river runoff in the mid-latitudes. *Wageningen University & Research*. <https://doi.org/10.18174/529303>
- Climate-data.org. (n.d.). *CLIMA VALENCIA*. climate-data.org. Retrieved September 29, 2022, from <https://es.climate-data.org/europe/espana/comunidad-valenciana/valencia-845/>
- CLO. (2018, April 25). *Temperatuur in Nederland en mondiaal, 1906 - 2017*. Compendium Voor De Leefomgeving. Retrieved April 6, 2023, from <https://www.clo.nl/indicatoren/nl022613-temperatuur-mondiaal-en-in-nederland#:~:text=De%20lente%20en%20de%20zomer,1%2C0%20%C2%B0C%20gestegen.>
- Copernicus Climate Change Service. (2022). *Copernicus Climate Data Store* /. [cds.climate.copernicus.eu](https://cds.climate.copernicus.eu). Retrieved September 22, 2022, from

- <https://cds.climate.copernicus.eu/cdsapp#!/dataset/reanalysis-era5-pressure-levels?tab=form>
- ECMWF. (2022). *L137 model level definitions*. Confluence Ecmwf. Retrieved September 27, 2022, from <https://confluence.ecmwf.int/display/UDOC/L137+model+level+definitions>
- ECMWF. (2023, May 5). ERA5: uncertainty estimation. confluence.ecmwf.int. Retrieved May 16, 2023, from <https://confluence.ecmwf.int/display/CKB/ERA5%3A+uncertainty+estimation>
- European Climate Assessment & Dataset. (2022). *E-OBS gridded dataset*. Retrieved September 27, 2022, from <https://www.ecad.eu/download/ensembles/download.php#datafiles>
- Ferreira, R. N. (2021, June 28). *Cut-Off Lows and Extreme Precipitation in Eastern Spain: Current and Future Climate*. MDPI. Retrieved September 19, 2022, from <https://www.mdpi.com/2073-4433/12/7/835>
- FloodList News. (2019, September 13). *3 Die in Floods After Torrential Rainfall in South East*. Retrieved October 18, 2022, from <https://floodlist.com/europe/spain-valencia-murcia-andalusia-and-castilelamancha-september-2019>
- Fosser, G., Khodayar, S., & Berg, P. (2014). Benefit of convection permitting climate model simulations in the representation of convective precipitation. *Climate Dynamics*, 44(1–2), 45–60. <https://doi.org/10.1007/s00382-014-2242-1>
- GloH2O. (2022). *MSWEP*. GloH2O. Retrieved September 22, 2022, from <http://www.gloh2o.org/mswep/>
- Grams, C. M., Binder, H., Pfahl, S., Piaget, N., & Wernli, H. (2014). Atmospheric processes triggering the central European floods in June 2013. *Natural Hazards and Earth System Sciences*, 14(7), 1691–1702. <https://doi.org/10.5194/nhess-14-1691-2014>
- Hersbach, H., Bell, B., Berrisford, P., Hirahara, S., Horányi, A., Muñoz-Sabater, J., Nicolas, J., Peubey, C., Radu, R., Schepers, D., Simmons, A., Soci, C., Abdalla, S., Abellan, X., Balsamo, G., Bechtold, P., Biavati, G., Bidlot, J., Bonavita, M., . . . Thépaut, J. (2020a). The ERA5 global

- reanalysis. *Quarterly Journal of the Royal Meteorological Society*, 146(730), 1999–2049.  
<https://doi.org/10.1002/qj.3803>
- Hersbach, H., Bell, B., Berrisford, P., Hirahara, S., Horányi, A., Muñoz-Sabater, J., Nicolas, J., Peubey, C., Radu, R., Schepers, D., Simmons, A., Soci, C., Abdalla, S., Abellan, X., Balsamo, G., Bechtold, P., Biavati, G., Bidlot, J., Bonavita, M., . . . Thépaut, J. (2020b). The ERA5 global reanalysis. *Quarterly Journal of the Royal Meteorological Society*, 146(730), 1999–2049.  
<https://doi.org/10.1002/qj.3803>
- IPCC. (2021). *IPCC Sixth Assessment Report*. Chapter 11: Weather and Climate Extreme Events in a Changing Climate. Retrieved April 6, 2023, from  
<https://www.ipcc.ch/report/ar6/wg1/chapter/chapter-11/>
- Jiang, Q., Li, W., Fan, Z., He, X., Sun, W., Chen, S., Wen, J., Gao, J., & Wang, J. (2021). Evaluation of the ERA5 reanalysis precipitation dataset over Chinese Mainland. *Journal of Hydrology*, 595, 125660. <https://doi.org/10.1016/j.jhydrol.2020.125660>
- Llasat, M. C., Martín, F., & Barrera, A. (2006). From the concept of “Kaltlufttropfen” (cold air pool) to the cut-off low. The case of September 1971 in Spain as an example of their role in heavy rainfalls. *Meteorology and Atmospheric Physics*, 96(1–2), 43–60.  
<https://doi.org/10.1007/s00703-006-0220-9>
- Miró-Granada Gelabert, J. (2013, October 20). *Una implicación jurídica de una predicción meteorológica sobre lluvias catastróficas*. Tiempo.com | Meteored. Retrieved September 21, 2022, from <https://www.tiempo.com/ram/639/una-implicacion-juridica-de-una-prediccion-meteorologica-sobre-lluvias-catastroficas-i/>
- Nieto, R., Gimeno, L., De La Torre, L., Ribera, P., Gallego, D., García-Herrera, R., García, J. A., Nuñez, M., Redaño, A., & Lorente, J. (2005). Climatological Features of Cutoff Low Systems in the Northern Hemisphere. *Journal of Climate*, 18(16), 3085–3103.  
<https://doi.org/10.1175/jcli3386.1>



- Nieto, R., Sprenger, M., Wernli, H., & Trigo, R. M. (2008). Identification and Climatology of Cut-off Lows near the Tropopause. *Annals of the New York Academy of Sciences*.  
<https://doi.org/10.1196/annals.1446.016>
- NOAA's National Weather Service. (n.d.). *Cutoff Low*. forecast.weather.gov. Retrieved September 20, 2022, from <https://forecast.weather.gov/glossary.php?word=cutoff%20low>
- Smit, P. (2022, February 4). *Wat als Limburgse 'waterbom' elders boven Nederland was gevallen?* Alpenweerman. Retrieved September 21, 2022, from <https://www.alpenweerman.nl/klimaat-wat-als-limburgse-waterbom-elders-boven-nederland-was-gevallen/>
- Sodemann, H., Schwierz, C., & Wernli, H. (2008). Interannual variability of Greenland winter precipitation sources: Lagrangian moisture diagnostic and North Atlantic Oscillation influence. *Journal of Geophysical Research*, 113(D3). <https://doi.org/10.1029/2007jd008503>
- Sprenger, M., & Wernli, H. (2015). The LAGRANTO Lagrangian analysis tool – version 2.0. *Geoscientific Model Development*, 8(8), 2569–2586. <https://doi.org/10.5194/gmd-8-2569-2015>
- Temperatuur in Nederland en mondiaal, 1906 - 2017 | Compendium voor de Leefomgeving*. (n.d.). <https://www.clo.nl/indicatoren/nl022613-temperatuur-mondiaal-en-in-nederland#:~:text=De%20lente%20en%20de%20zomer,1%2C0%20%C2%B0C%20gestegen.>
- Tompkins, A. M. (2001, March 1). *Organization of Tropical Convection in Low Vertical Wind Shears: The Role of Water Vapor*. <https://journals.ametsoc.org/>. Retrieved September 20, 2022, from [https://journals.ametsoc.org/view/journals/atsc/58/6/1520-0469\\_2001\\_058\\_0529\\_oocil\\_2.0.co\\_2.xml](https://journals.ametsoc.org/view/journals/atsc/58/6/1520-0469_2001_058_0529_oocil_2.0.co_2.xml)

## Figures

- AEMET. (n.d.). *Standard climate Values - State Meteorological Agency - AEMET - Spanish Government*. State Meteorological Agency - AEMET - Spanish Government. Retrieved March

28, 2023, from

<https://www.aemet.es/en/serviciosclimaticos/datosclimatologicos/valoresclimatologicos>

De Meteorology A, A. E. (n.d.). *Standard climate Values - State Meteorological Agency - AEMET -*

*Spanish Government*. State Meteorological Agency - AEMET - Spanish Government.

<https://www.aemet.es/en/serviciosclimaticos/datosclimatologicos/valoresclimatologicos>

Nieto, R., Sprenger, M., Wernli, H., & Trigo, R. M. (2008). Identification and Climatology of Cut-off Lows near the Tropopause. *Annals of the New York Academy of Sciences*.

<https://doi.org/10.1196/annals.1446.016>

Ocean Navigator. (2017, March 30). *The cut-off low*. Retrieved September 20, 2022, from

<https://oceannavigator.com/the-cut-off-low/>

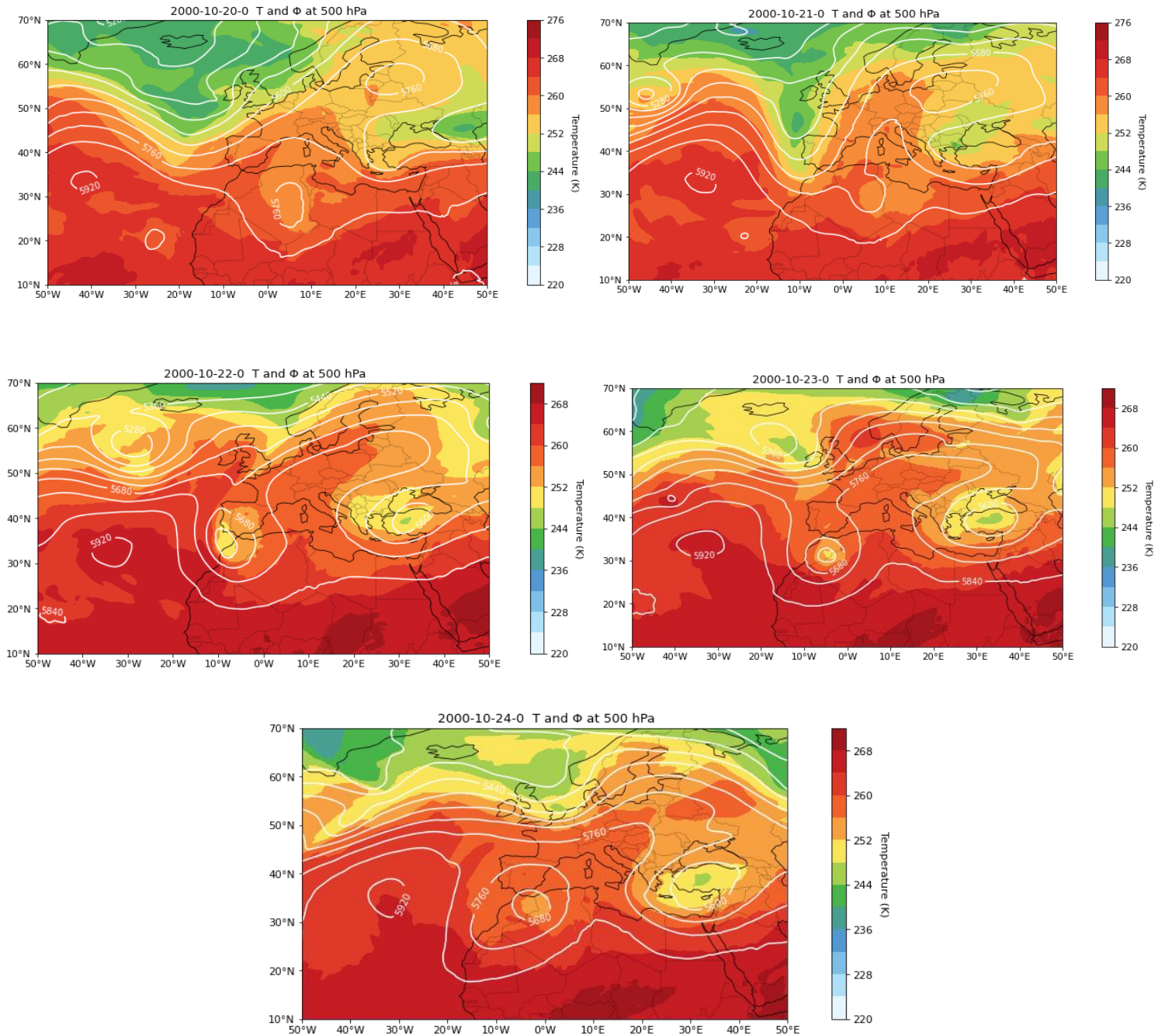
Racicot, A. (2022). *bbox finder*. Bboxfinder. Retrieved September 27, 2022, from

<http://bboxfinder.com/#38.000000,-1.000000,40.000000,1.000000>

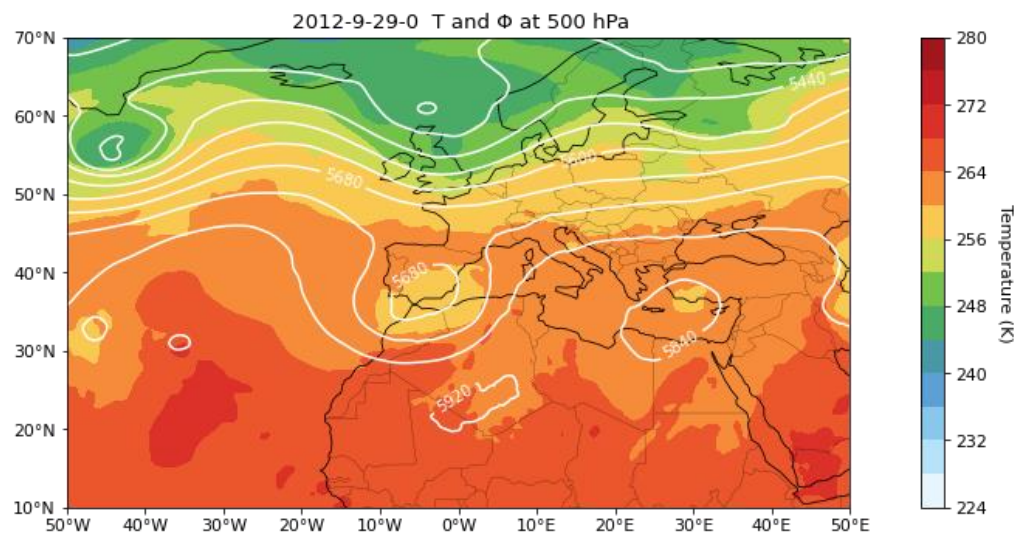
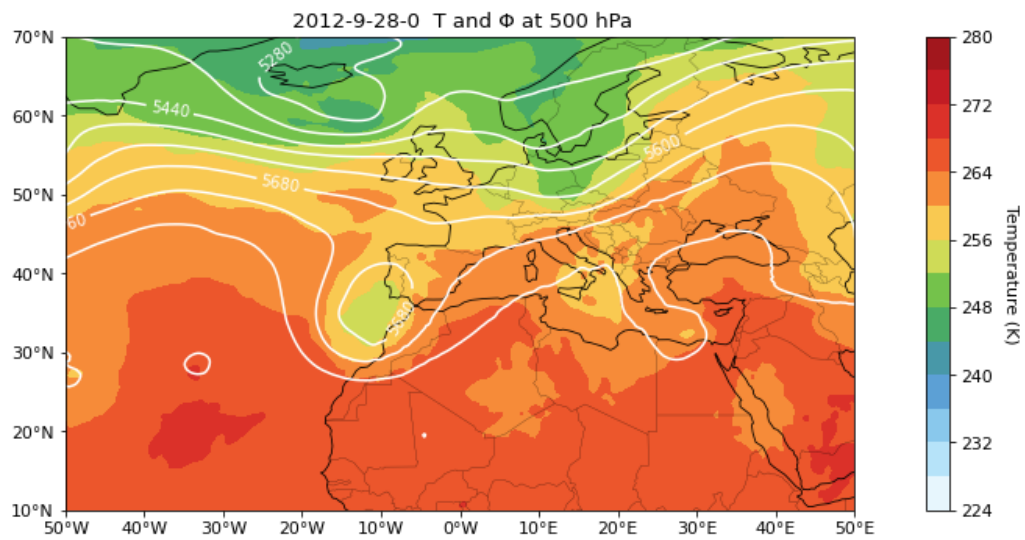
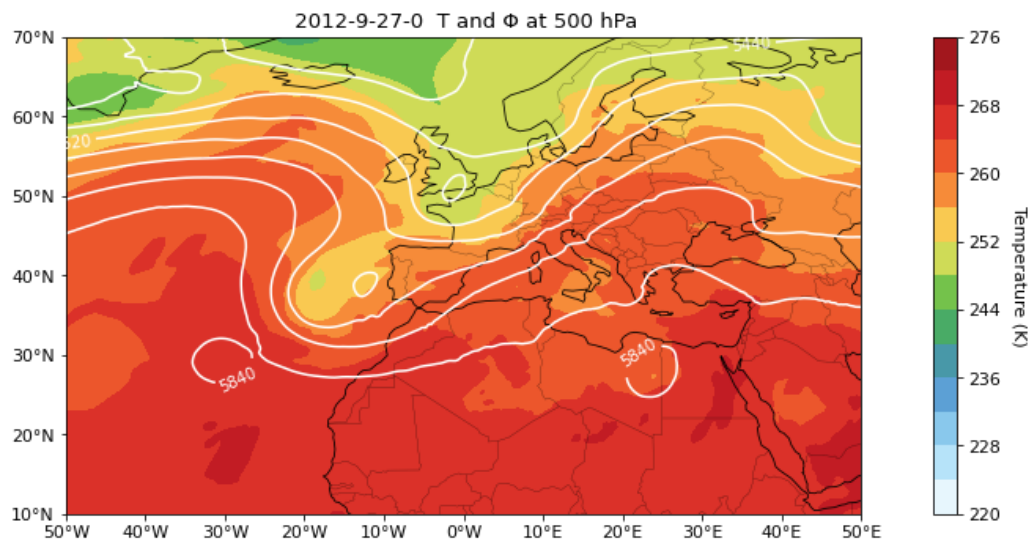
## Appendix A - Synoptic weather situation

The Synoptic weather situation in terms of geopotential height and the temperature at 500 hPa for the cases in 2000, 2012 and 2019.

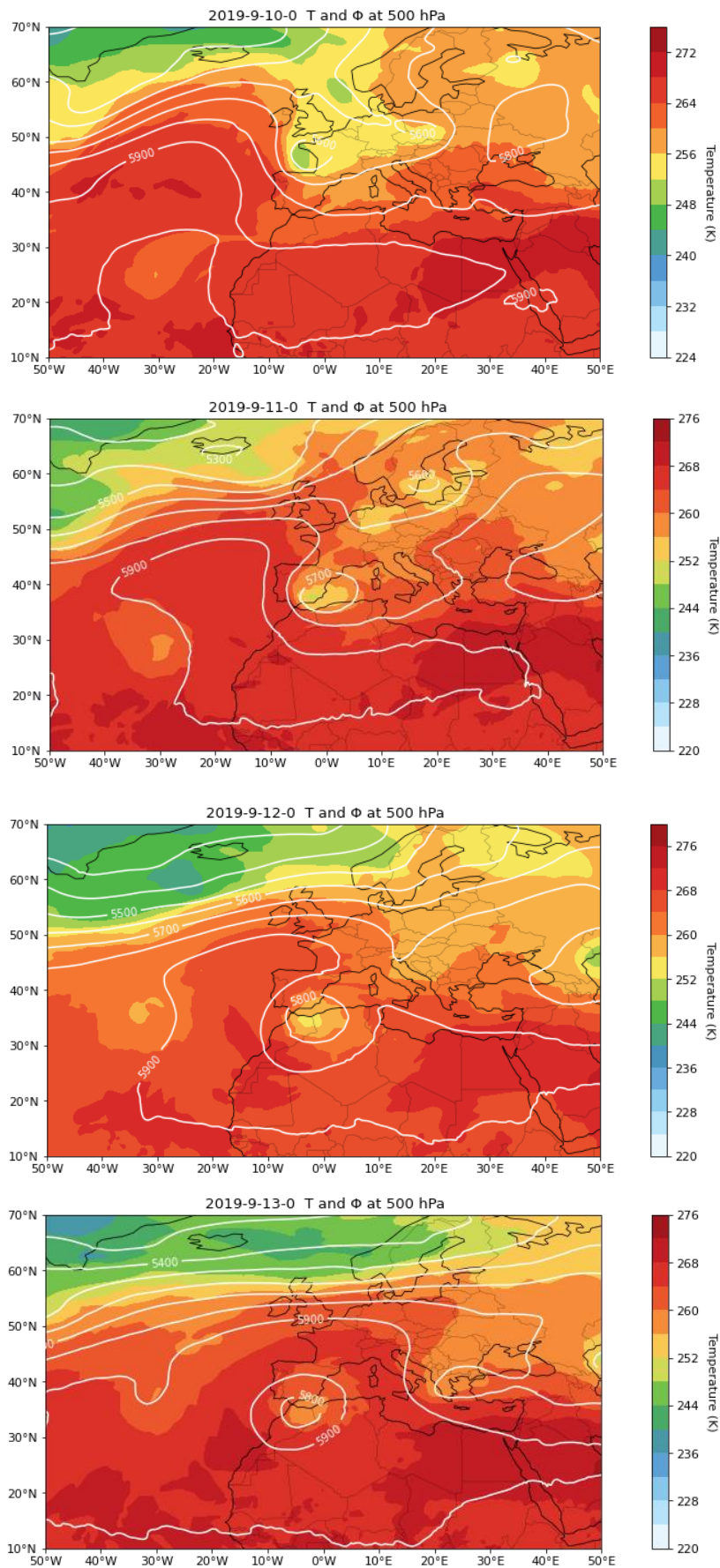
### Geopotential & temperature at 500 hPa 2000



## Geopotential & temperature at 500 hPa 2012



## Geopotential & temperature at 500 hPa 2019



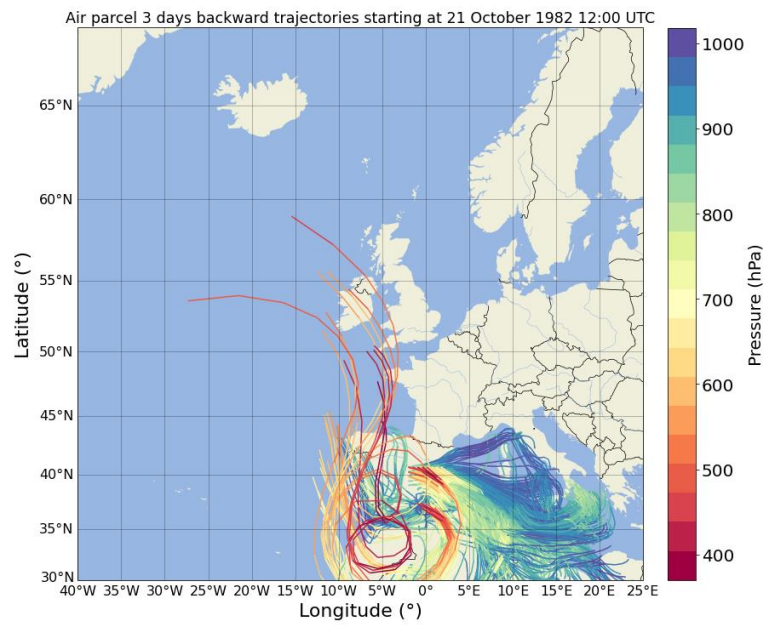
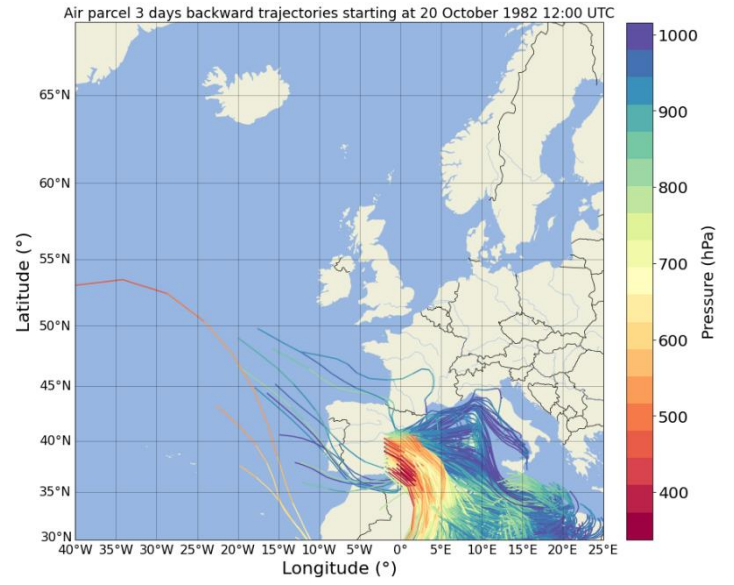
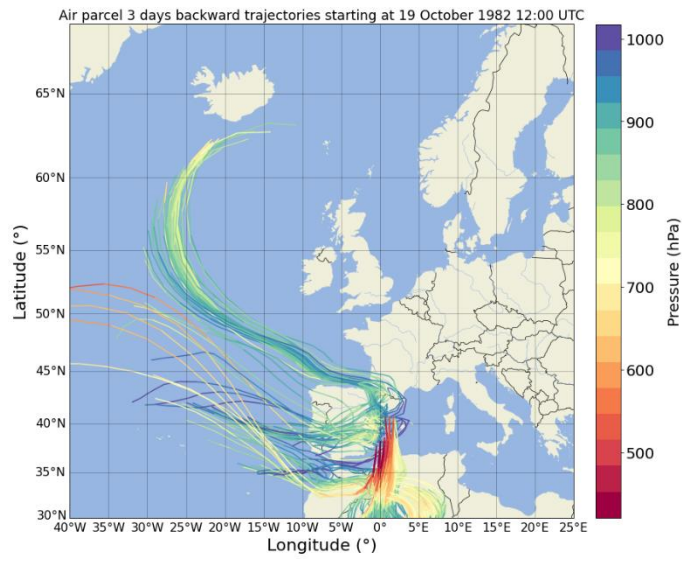


## Appendix B - Air parcel trajectories

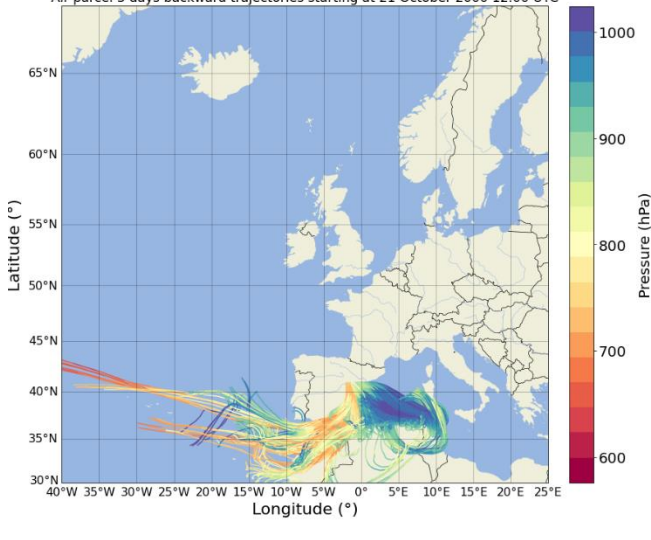
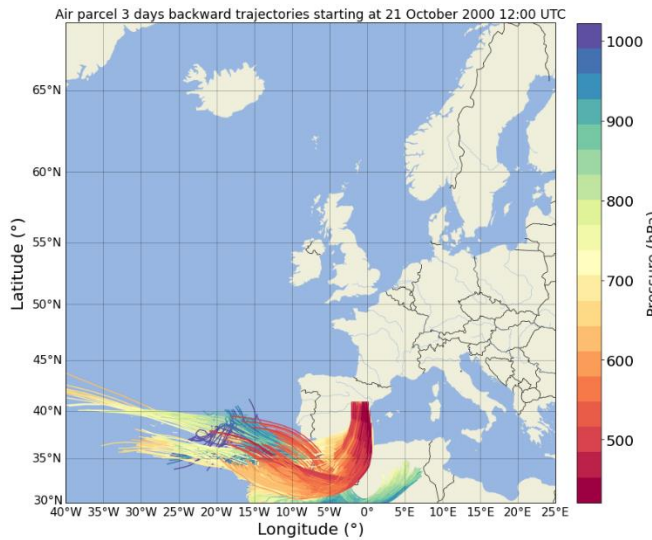
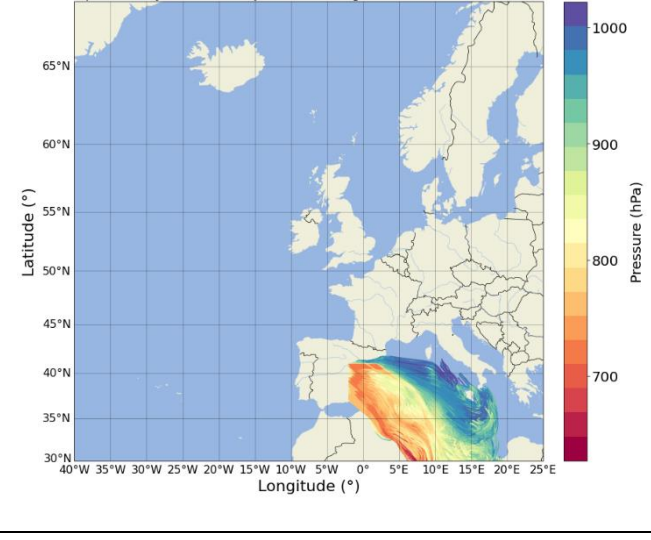
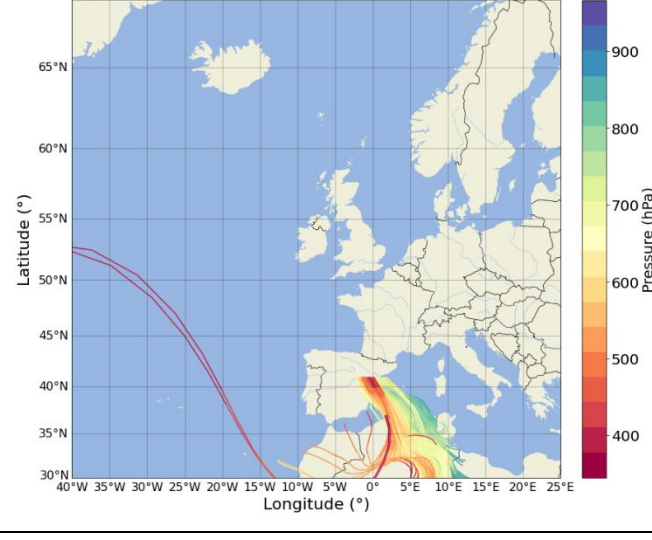
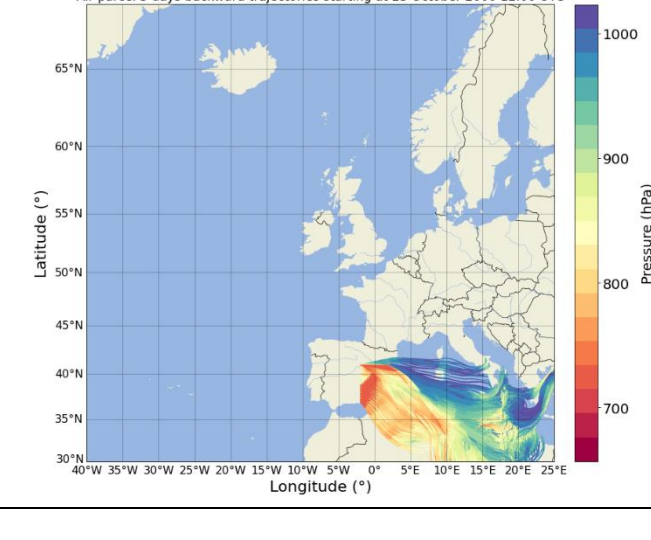
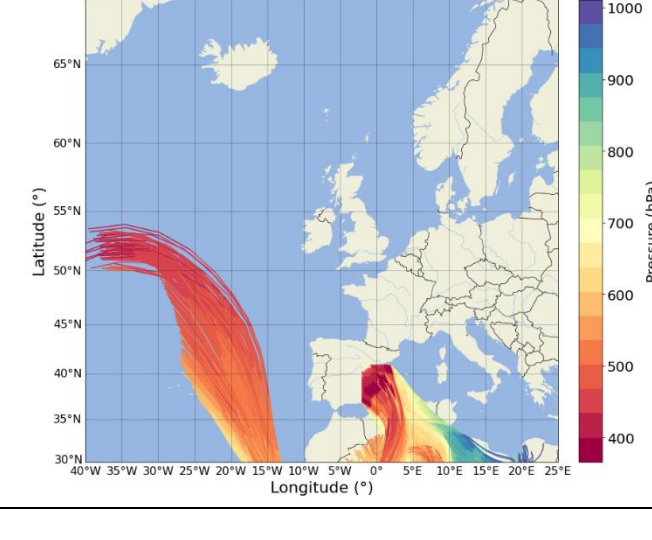
Obtained with LAGRANTO

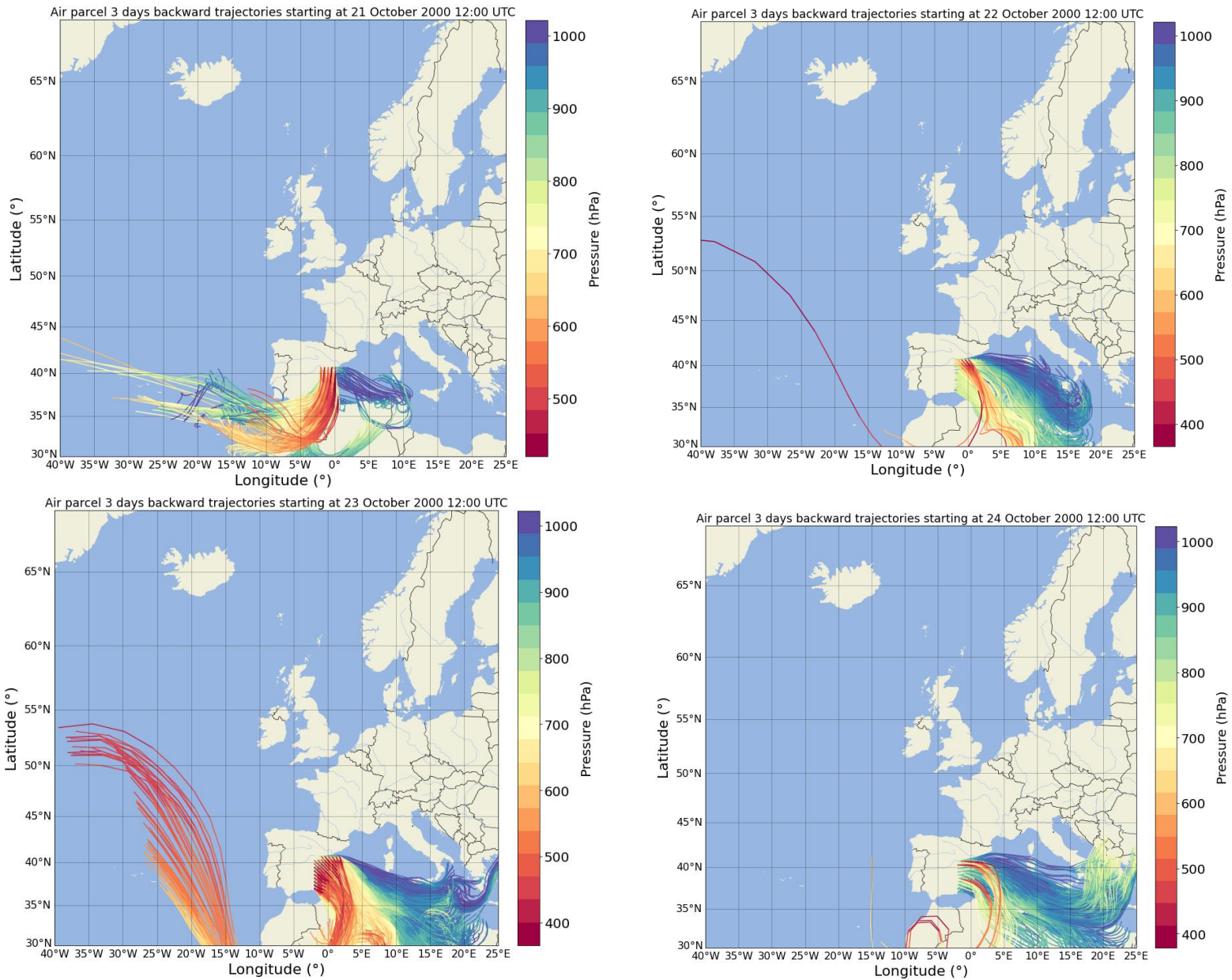
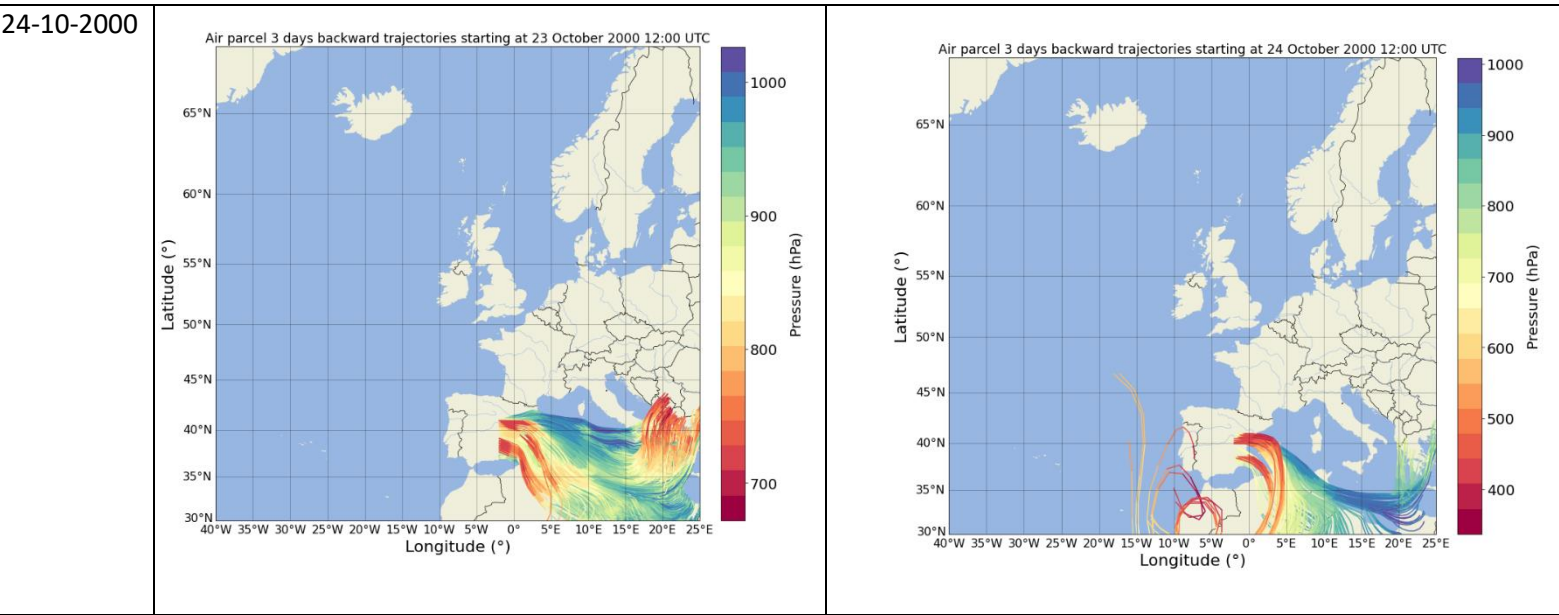
Date	>700 hPa (1050 – 700 hPa)	>700 hPa (700 – 400 hPa)
19-10-1982	<p>Air parcel 3 days backward trajectories starting at 19 October 1982 12:00 UTC</p>	<p>Air parcel 3 days backward trajectories starting at 19 October 1982 12:00 UTC</p>
20-10-1982	<p>Air parcel 3 days backward trajectories starting at 20 October 1982 12:00 UTC</p>	<p>Air parcel 3 days backward trajectories starting at 20 October 1982 12:00 UTC</p>
21-10-1982	<p>Air parcel 3 days backward trajectories starting at 21 October 1982 12:00 UTC</p>	<p>Air parcel 3 days backward trajectories starting at 21 October 1982 12:00 UTC</p>

Spacing = 45 km + selections (RH =>80% and DeltaQ=<0)

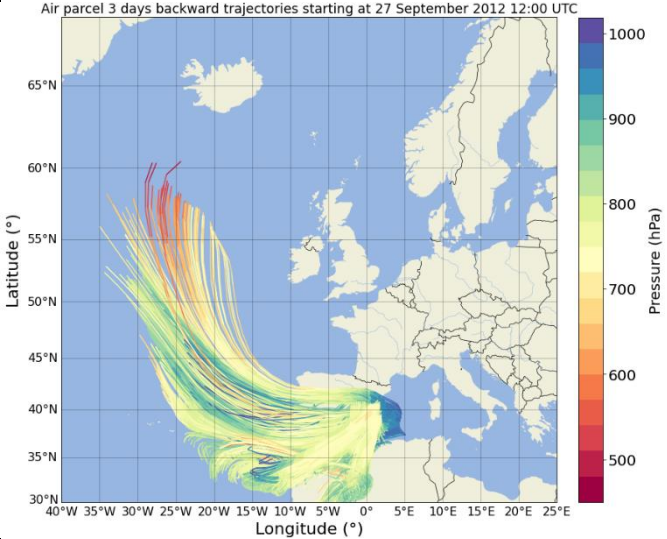
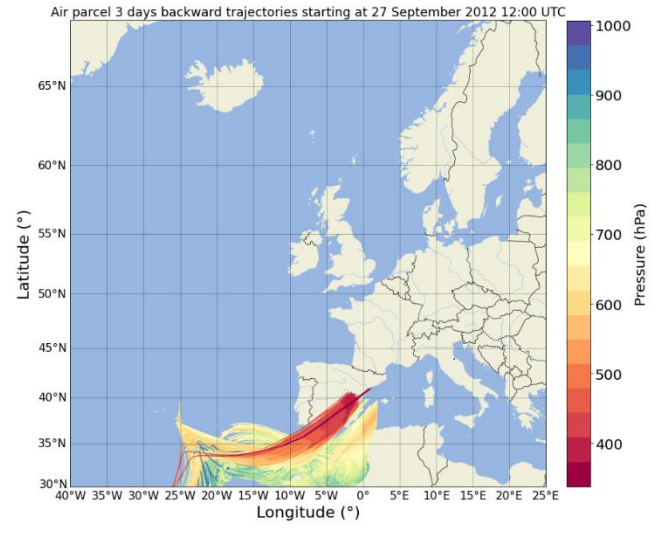
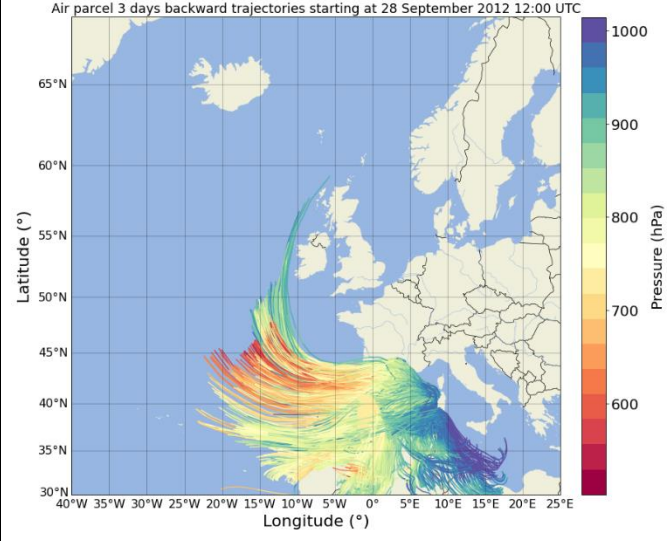
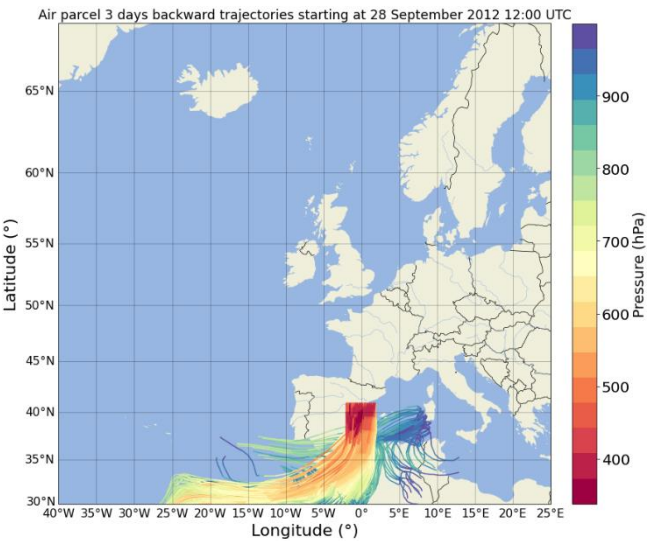
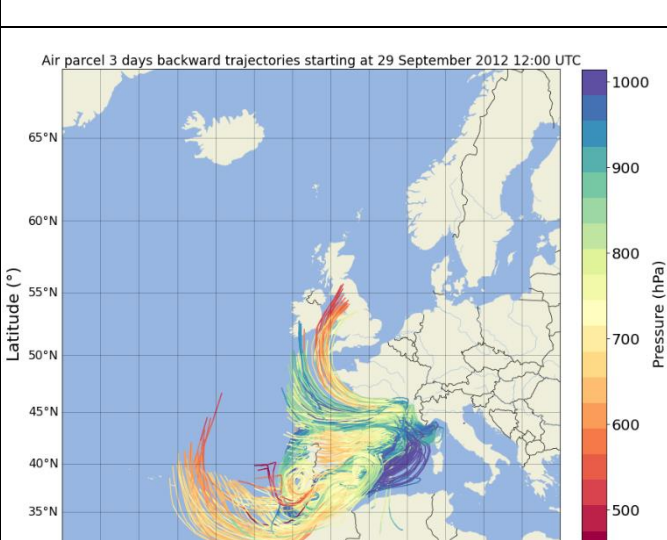
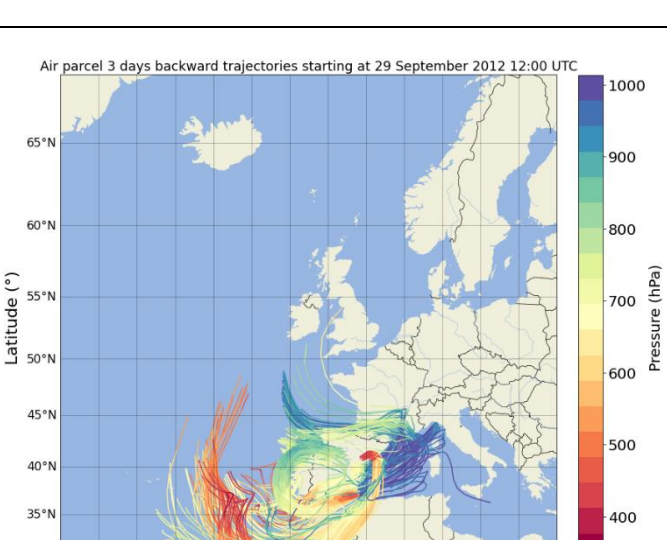


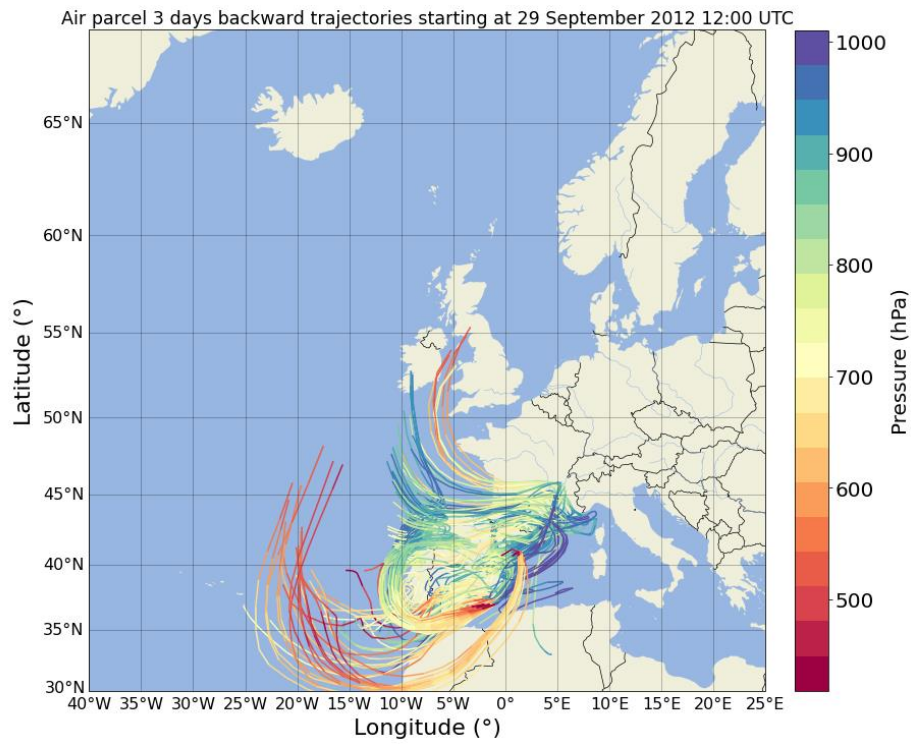
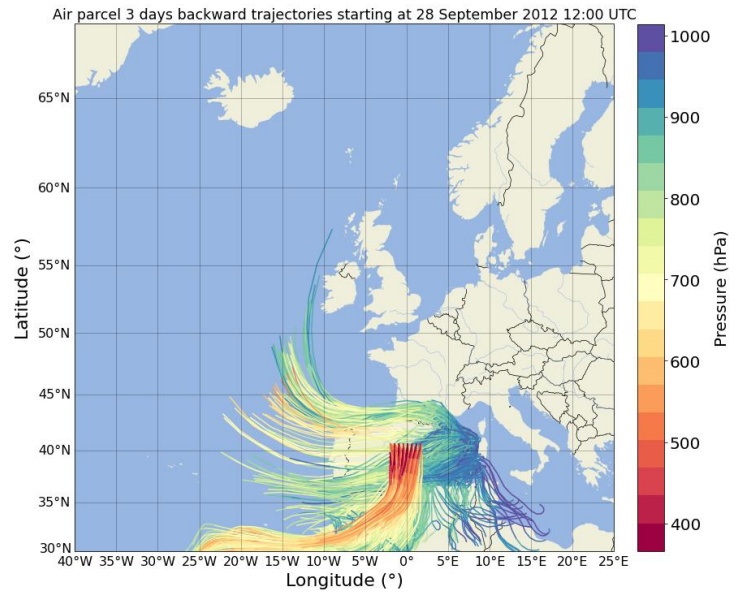
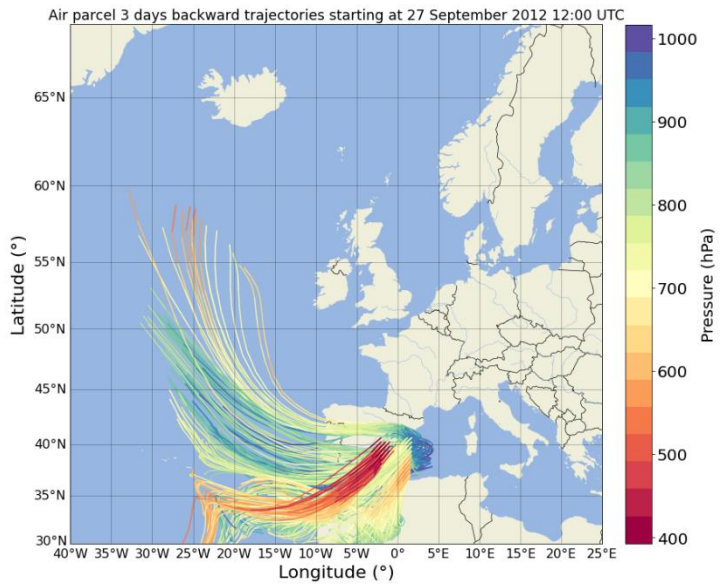


Date	>700 hPa (1050 – 700 hPa)	>700 hPa (700 – 400 hPa)
21-10-2000	<p>Air parcel 3 days backward trajectories starting at 21 October 2000 12:00 UTC</p> 	<p>Air parcel 3 days backward trajectories starting at 21 October 2000 12:00 UTC</p> 
22-10-2000	<p>Air parcel 3 days backward trajectories starting at 22 October 2000 12:00 UTC</p> 	<p>Air parcel 3 days backward trajectories starting at 22 October 2000 12:00 UTC</p> 
23-10-2000	<p>Air parcel 3 days backward trajectories starting at 23 October 2000 12:00 UTC</p> 	<p>Air parcel 3 days backward trajectories starting at 23 October 2000 12:00 UTC</p> 

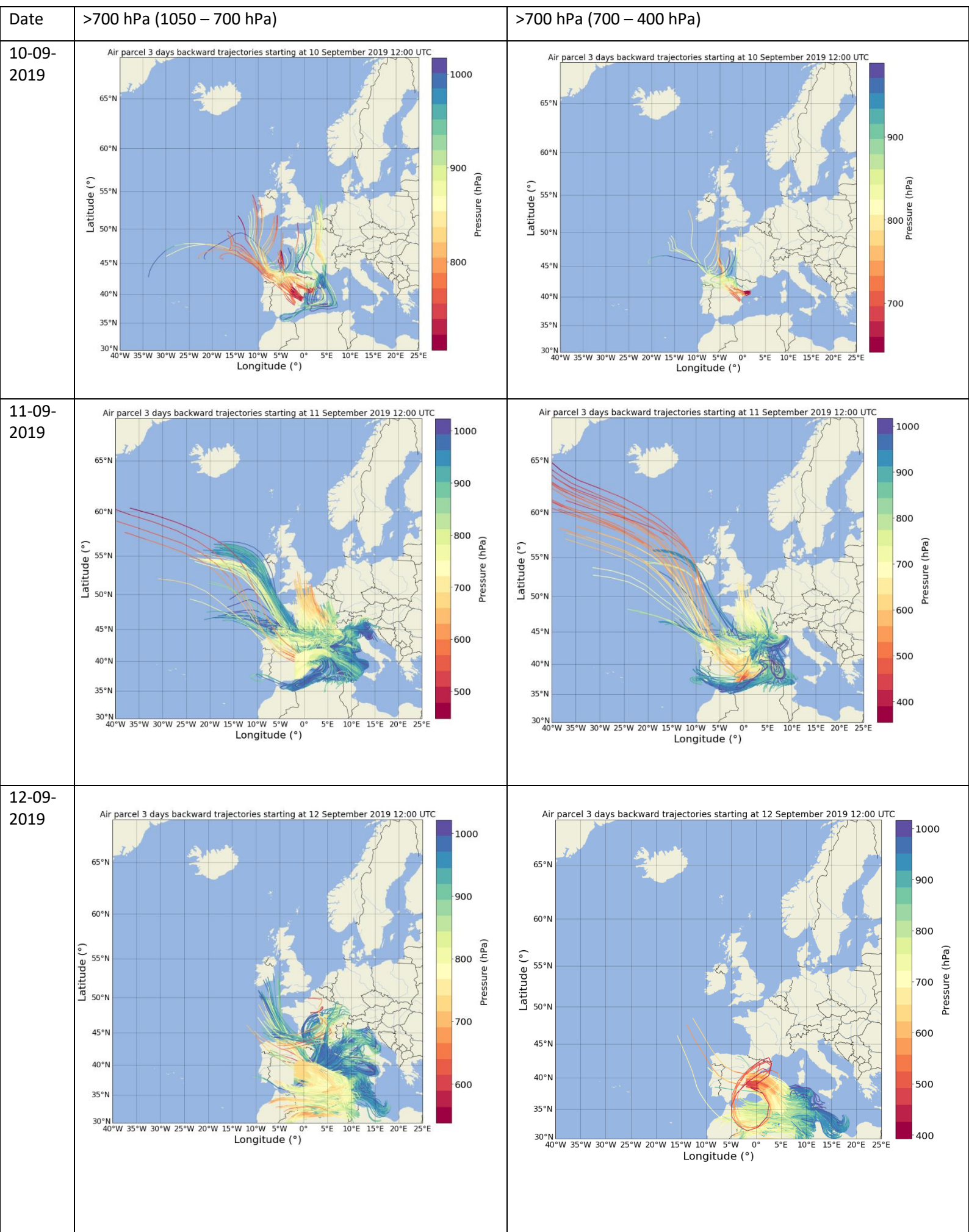




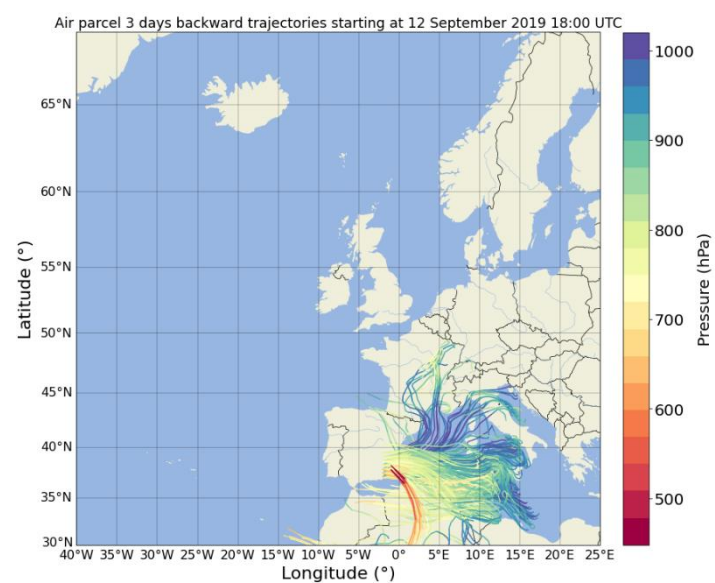
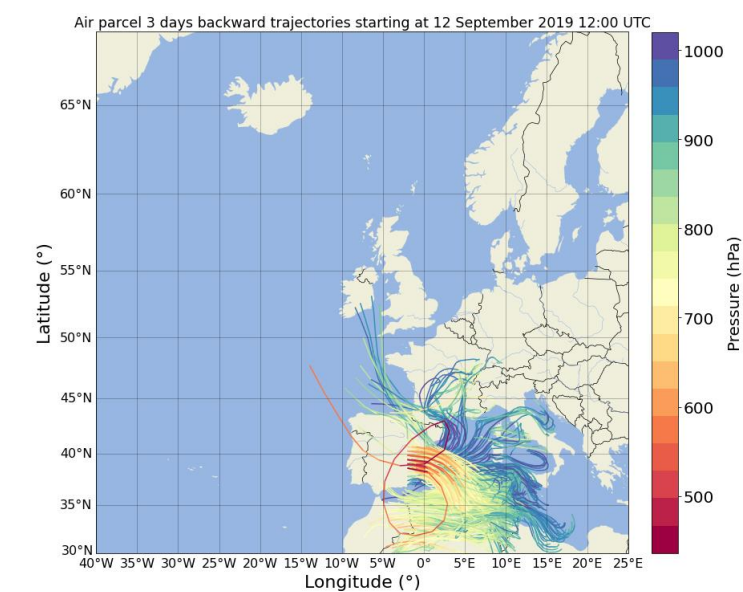
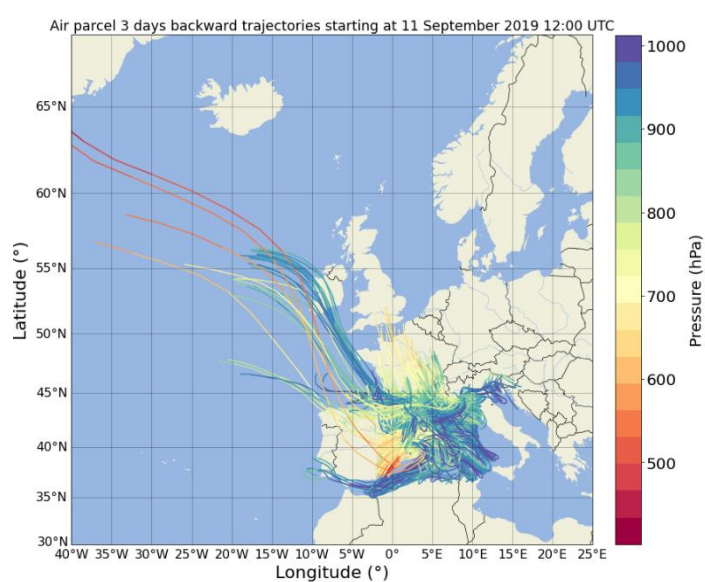
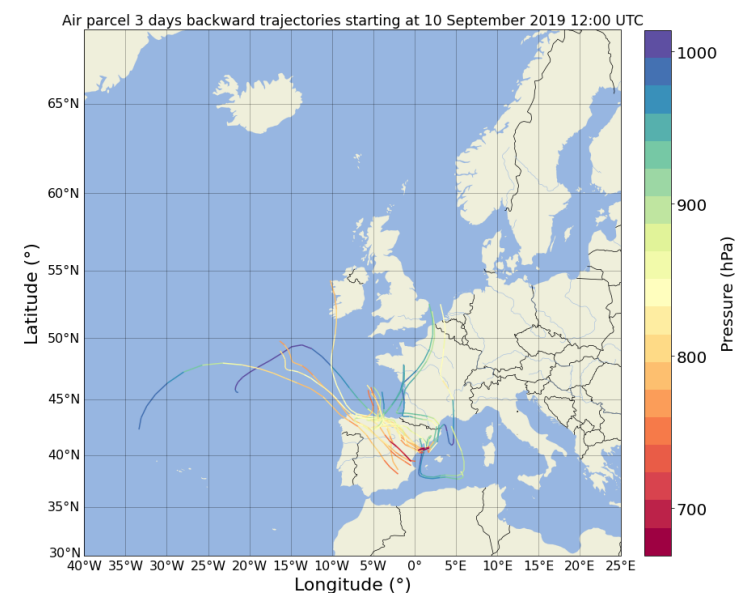
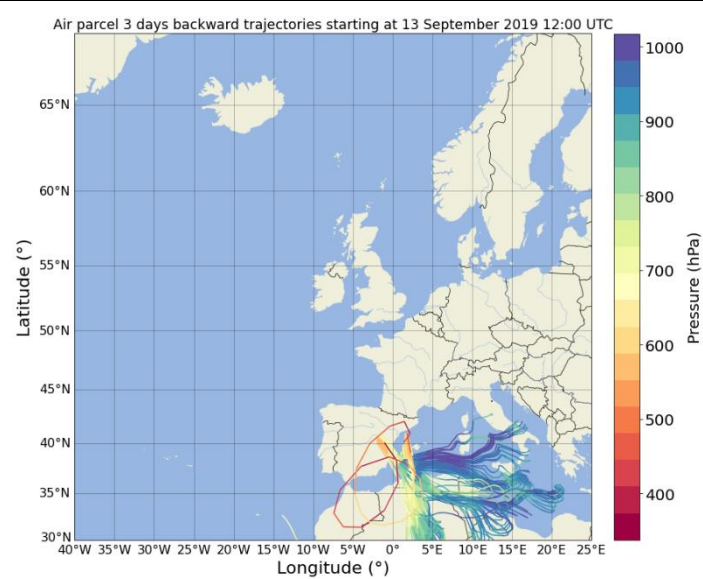
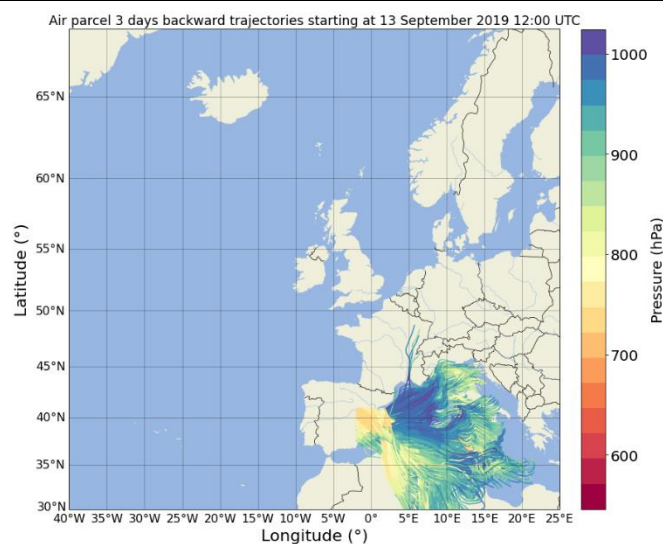
Date	>700 hPa (1050 – 700 hPa)	>700 hPa (700 – 400 hPa)
27-09-2012	<p>Air parcel 3 days backward trajectories starting at 27 September 2012 12:00 UTC</p> 	<p>Air parcel 3 days backward trajectories starting at 27 September 2012 12:00 UTC</p> 
28-09-2012	<p>Air parcel 3 days backward trajectories starting at 28 September 2012 12:00 UTC</p> 	<p>Air parcel 3 days backward trajectories starting at 28 September 2012 12:00 UTC</p> 
29-09-2012	<p>Air parcel 3 days backward trajectories starting at 29 September 2012 12:00 UTC</p> 	<p>Air parcel 3 days backward trajectories starting at 29 September 2012 12:00 UTC</p> 







13-09-  
2019

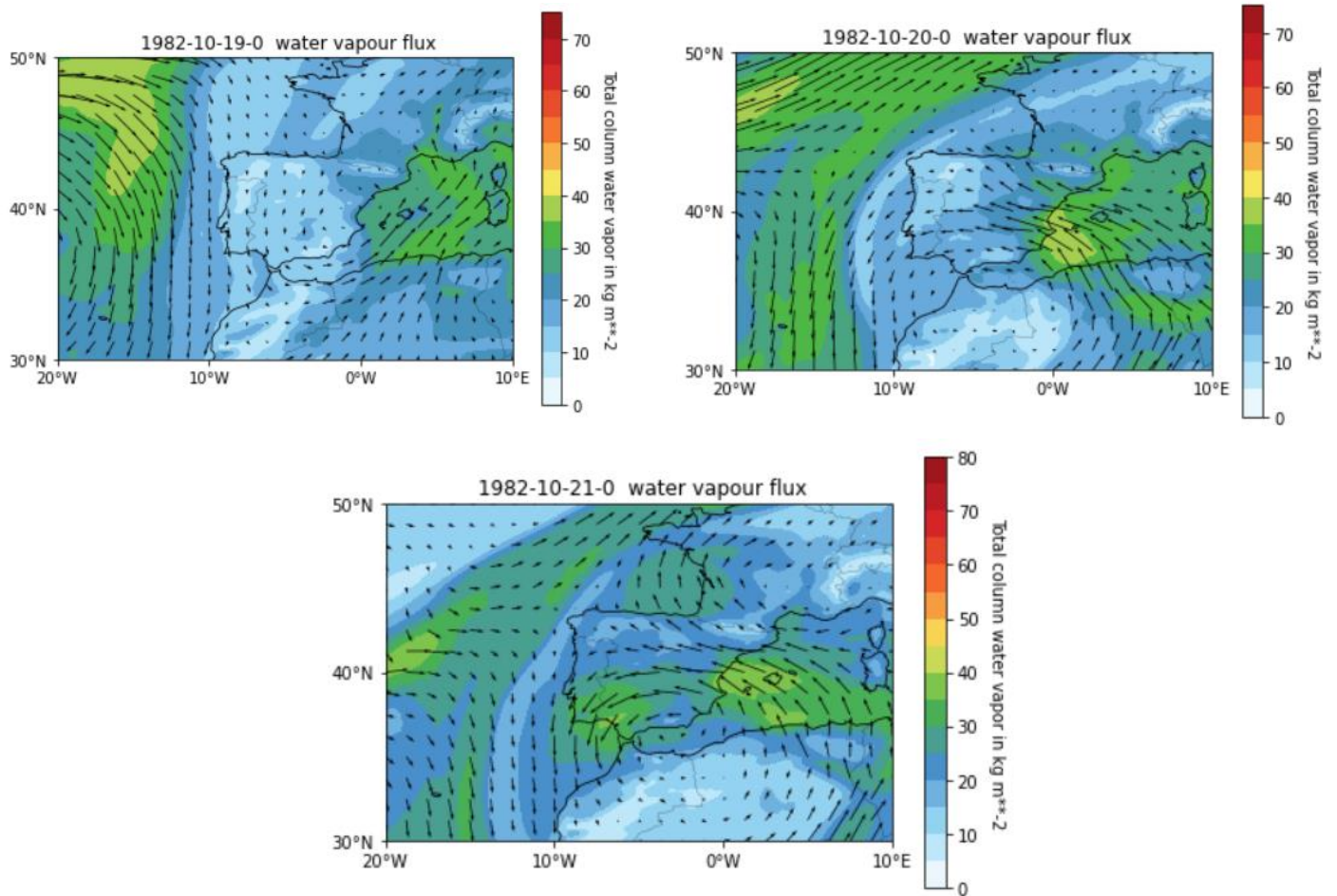




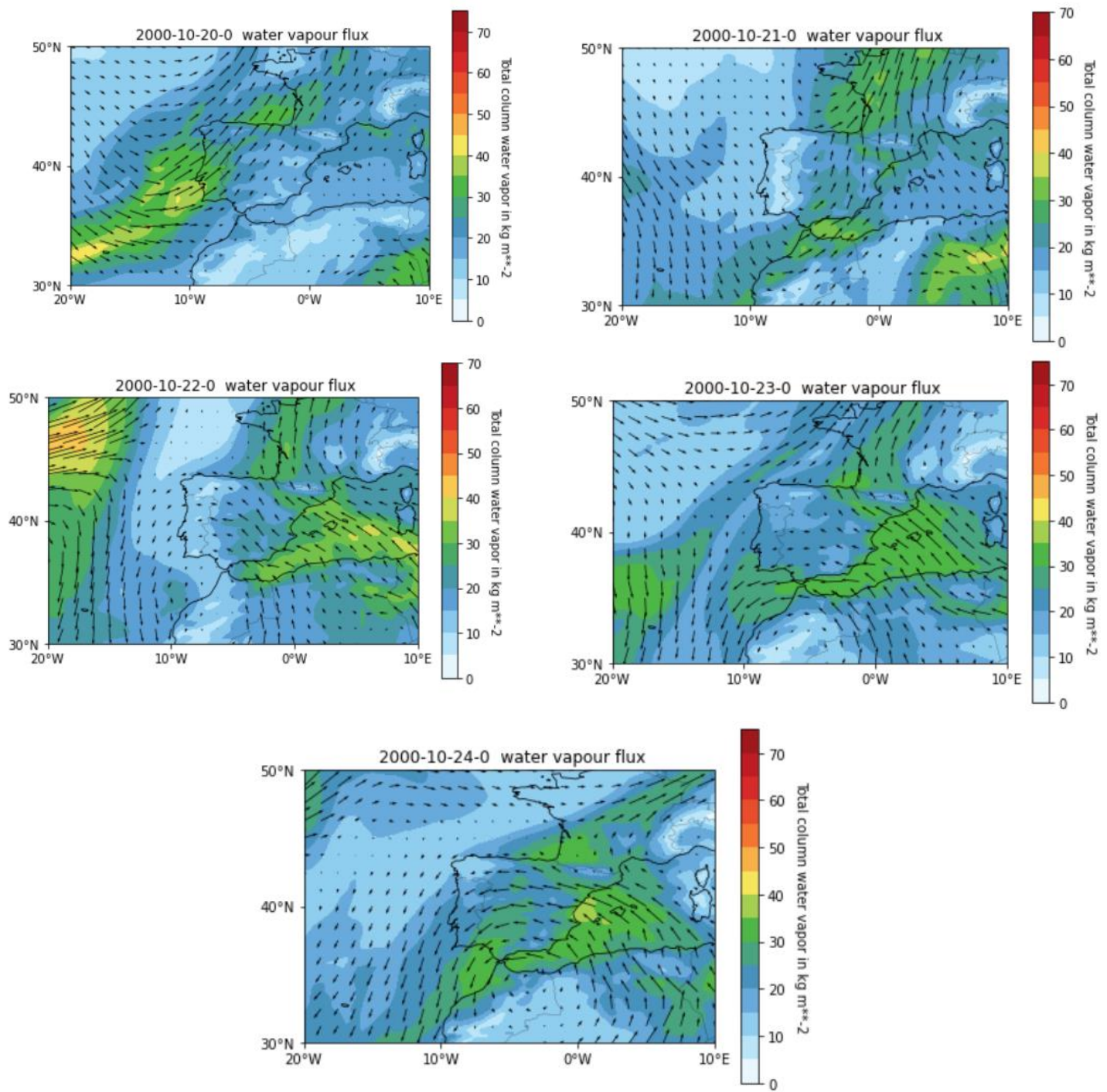
## Appendix C – Water vapour fluxes

Vertical integral of water vapour flux over Southwest Europe at different time steps for 1982, 2000, 2012 and 2019.

**1982**

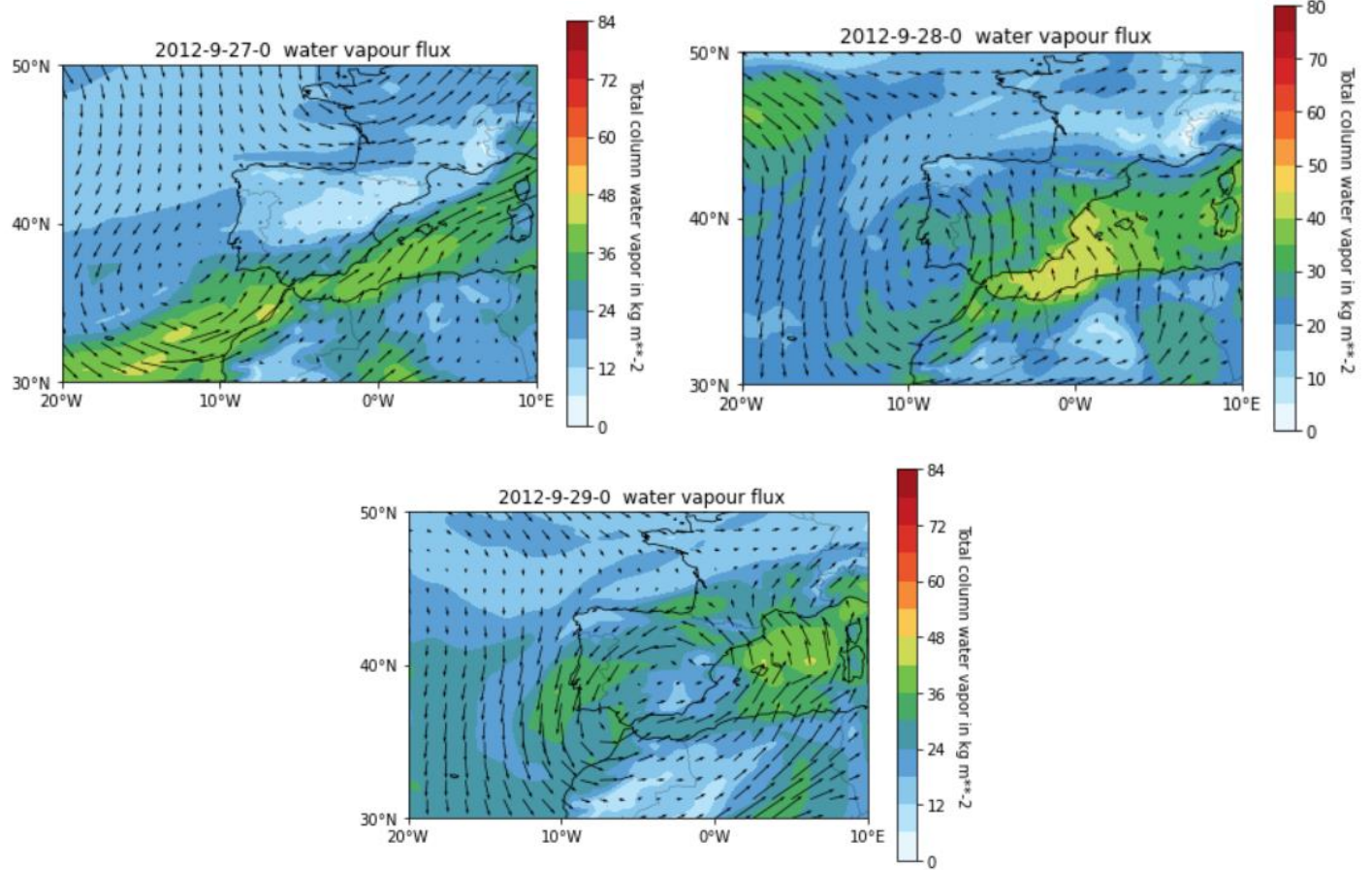


2000





2012



2019

